American Journal of Advanced Technology and Engineering Solutions

Volume: 6; **Issue:** 1
Pages: 228-266
eISSN: 3067-5146

open access

Crossref

DEEP LEARNING–ENABLED LIDAR AND MULTISPECTRAL SIGNATURE FUSION FOR FLOOD HAZARD MAPPING AND LAND-SURFACE VULNERABILITY PREDICTION

Ratul Debnath[1];

[1]. GIS Pipeline Integrity Analyst, Centric Infrastructure Group, The Woodlands, Texas, USA; Email: ratuldebnathgis@gmail.com

Doi: 10.63125/6mc3v739
Received: 12 October 2025; **Revised:** 22 November 2025; **Accepted:** 20 December 2025; **Published:** 10 January 2026

Abstract

This study developed and validated a quantitative flood hazard and land-surface vulnerability modeling framework that integrated LiDAR-derived terrain information with multispectral surface-condition signatures using deep learning and benchmark statistical approaches. Flood vulnerability was operationalized as a continuous, probability-like spatial outcome, and model performance was evaluated under a decision-utility framework that emphasized discrimination, calibration, and ranking quality in a rare-event setting. The analysis was conducted using a retrospective observational design applied to a finalized dataset of approximately 1.25 million raster cells, of which 62,500 (5.0%) were labeled as flood-positive based on event-linked inundation references. The dataset was partitioned into training (70%), validation (15%), and holdout test (15%) subsets using spatially disciplined splits to reduce leakage from spatial autocorrelation. Descriptive results indicated that flood-positive observations were concentrated in low-elevation, low-slope, high-convergence terrain and were more frequently associated with elevated imperviousness and wetness signatures. Reliability analysis showed acceptable internal consistency for composite predictor constructs, with Cronbach's alpha values ranging from 0.75 to 0.86 across terrain and multispectral feature families. Baseline regression modeling confirmed statistically significant associations for all major construct families, with the strongest effects observed for convergence and wetness proxies and negative associations for elevation and slope structure. Comparative model evaluation demonstrated that non-linear approaches outperformed the regression benchmark. The fused LiDAR–multispectral convolutional neural network achieved the highest discrimination on the holdout test set, with an AUC-ROC of 0.94 and an AUC-PR of 0.63, compared with 0.84 and 0.41, respectively, for the regression baseline. Calibration quality also improved, as reflected by a lower Brier score (0.084 versus 0.118) and reduced expected calibration error (0.025 versus 0.041). Ranking utility gains were substantial, with precision at the top 1% of ranked locations increasing from 0.34 for regression to 0.52 for the fused model, and top-decile capture improving from 0.52 to 0.74 while reducing false alerts from 620 to 470 per 10,000 evaluated cells. Robustness testing across regional, catchment, and terrain-class holdouts confirmed that performance gains persisted under spatial generalization. Overall, the findings demonstrated that integrating LiDAR microtopography and multispectral surface-condition information through disciplined data fusion and spatially credible validation produced statistically robust and decision-useful flood vulnerability maps.

Keywords

Flood Hazard, Lidar, LiDAR, Multispectral Fusion, Deep Learning;

INTRODUCTION

Flood hazards represent one of the most persistent and destructive natural processes affecting human settlements, ecosystems, and economic systems at a global scale. Flooding is conventionally defined as the temporary inundation of normally dry land by water originating from rivers, coastal surges, intense precipitation, or infrastructure failure. In hazard science, flood risk is understood as a function of hazard intensity, exposure, and vulnerability, where vulnerability captures the susceptibility of land surfaces, infrastructure, and populations to flood-induced damage (Maranzoni et al., 2023).

Figure 1: Integrated Flood Hazard Mapping Framework

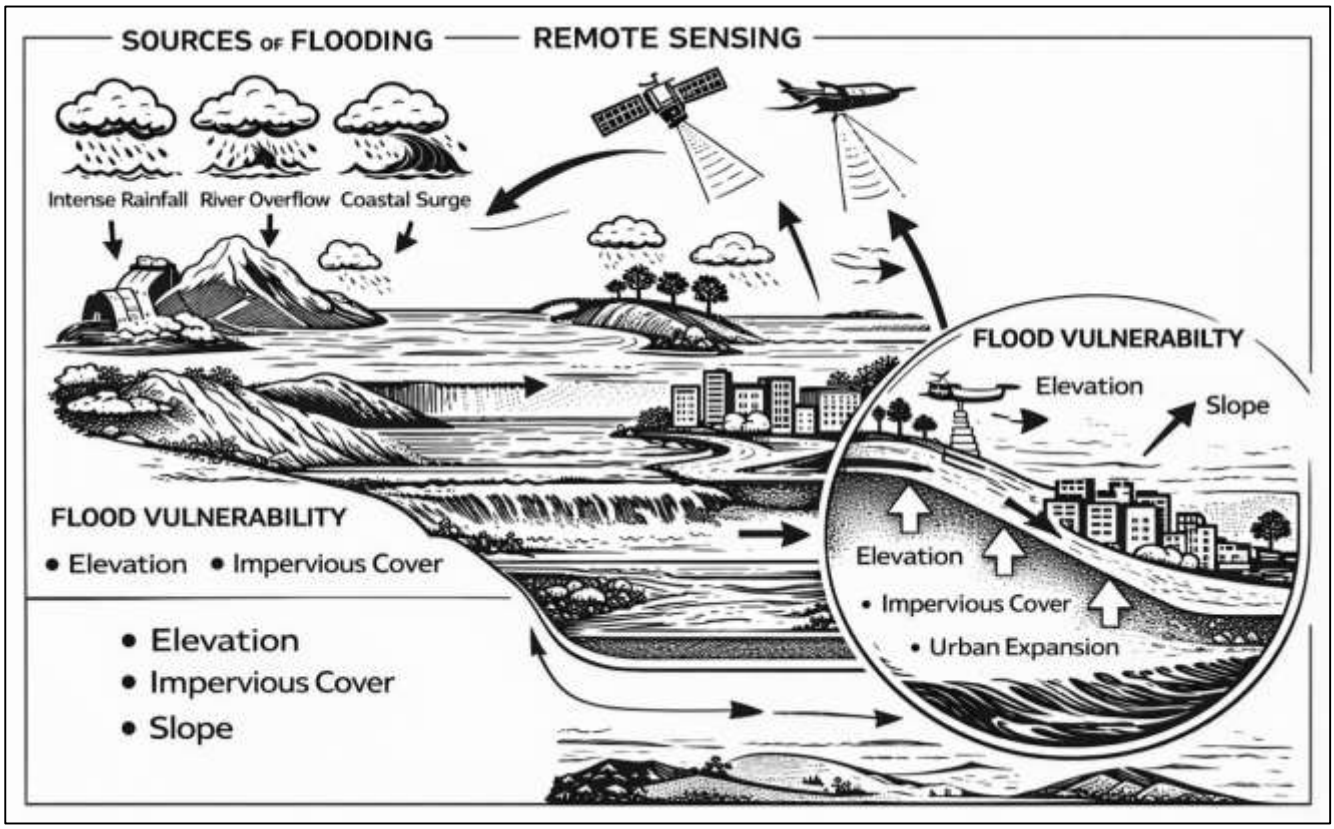

Land-surface vulnerability refers specifically to the physical and environmental characteristics that influence how terrain, soil, vegetation, and built environments respond to hydrological stress. These characteristics include elevation, slope, surface roughness, soil permeability, land-cover composition, and drainage connectivity. At an international level, flood vulnerability has become a central concern due to accelerating urbanization, land-use change, and climate-driven shifts in precipitation extremes that amplify surface runoff and inundation frequency across diverse geographic contexts. Global assessments by international agencies consistently report flooding as the most frequent and economically damaging natural hazard, with disproportionate impacts in low-lying coastal zones, riverine plains, and rapidly expanding urban regions (Kvočka et al., 2016). Quantitative flood hazard mapping therefore serves as a foundational instrument for disaster risk reduction, spatial planning, insurance modeling, and infrastructure design. Traditional flood mapping approaches have relied on hydrodynamic simulations, historical flood records, and manually derived terrain indicators. While effective in localized studies, these methods often struggle to scale across heterogeneous landscapes and data regimes. Advances in earth observation technologies have introduced new possibilities for representing land-surface properties with unprecedented spatial detail and temporal consistency. Within this evolving scientific context, flood hazard mapping is increasingly conceptualized as a spatial pattern recognition problem, where vulnerability emerges from measurable relationships between terrain morphology, surface composition, and hydrological processes (Kvočka et al., 2016). This reconceptualization has opened pathways for data-driven modeling frameworks capable of integrating

diverse geospatial signals into unified predictive representations.

Remote sensing has emerged as a cornerstone of modern flood hazard analysis due to its capacity to provide synoptic, repeatable, and spatially consistent observations across large geographic extents. Satellite-based sensing systems enable the extraction of land-surface attributes that directly influence flood behavior, including elevation gradients, surface roughness, vegetation density, impervious cover, and moisture dynamics (Kabenge et al., 2017). Optical multispectral sensors capture reflectance patterns across visible, near-infrared, and shortwave infrared bands, allowing quantitative discrimination of land-cover classes, vegetation health, soil exposure, and water bodies. These spectral signatures serve as proxies for infiltration capacity, runoff potential, and surface storage characteristics. Radar and microwave sensors complement optical data by penetrating cloud cover and providing sensitivity to surface moisture and roughness, which are critical during flood events. Over time, the integration of multi-sensor remote sensing data has enabled flood mapping efforts to transition from static cartographic products to dynamic spatial analyses (Qiang, 2019). International flood monitoring initiatives increasingly rely on satellite-derived indicators to assess hazard exposure in data-scarce regions where ground-based hydrological measurements are limited. Quantitative studies have demonstrated that multispectral indices derived from satellite imagery, such as vegetation and water indices, exhibit statistically significant associations with flood occurrence and extent. These associations support the use of spectral information as input variables for predictive modeling. However, multispectral data alone are constrained by limitations related to vertical accuracy and fine-scale terrain representation. Flood behavior is strongly governed by subtle elevation differences and micro-topographic features that may not be fully resolved through optical imagery. This limitation has motivated the incorporation of elevation-focused sensing technologies into flood hazard workflows. The convergence of spectral and topographic information within a single modeling framework reflects an evolving recognition that flood vulnerability is multidimensional and cannot be captured through a single data modality (Moftakhari et al., 2019). Quantitative fusion of remote sensing datasets has thus become a central methodological challenge in contemporary flood risk research.

Light Detection and Ranging (LiDAR) technology provides high-resolution three-dimensional representations of land surfaces by measuring the time delay of laser pulses reflected from the ground. LiDAR-derived digital elevation models (DEMs) have transformed flood hazard analysis by enabling precise characterization of terrain morphology, drainage pathways, and surface depressions that govern water accumulation and flow (Macchione et al., 2019). Elevation accuracy at sub-meter resolution allows quantitative identification of flood-prone zones that may be overlooked in coarser elevation datasets. Hydrological derivatives computed from LiDAR DEMs, including slope, curvature, flow direction, flow accumulation, and topographic wetness indices, have been shown to exhibit strong statistical relationships with inundation patterns. These derivatives capture the physical processes that influence surface runoff convergence and storage, providing mechanistic insight into flood susceptibility. In urban environments, LiDAR data enable explicit modeling of built structures, road embankments, and drainage modifications that alter natural flow paths. International flood studies increasingly rely on LiDAR-based terrain models to improve the reliability of floodplain delineation and depth estimation (Slater et al., 2015). However, LiDAR data acquisition remains uneven across regions due to cost and logistical constraints, leading to spatial disparities in data availability. From a modeling perspective, LiDAR-derived variables often exhibit high dimensionality and multicollinearity, complicating their integration into traditional statistical frameworks. These characteristics necessitate analytical approaches capable of learning complex, non-linear relationships between terrain features and flood outcomes. The increasing volume and resolution of LiDAR datasets have therefore shifted flood hazard mapping from deterministic rule-based modeling toward data-driven learning paradigms. Within this transition, LiDAR is no longer treated solely as a preprocessing input but as a core information source whose patterns must be jointly interpreted with other land-surface signals to accurately characterize vulnerability (Johnson et al., 2016).

Multispectral remote sensing contributes complementary information to LiDAR by capturing the biochemical and compositional properties of land surfaces that regulate hydrological response. Surface reflectance patterns encode vegetation structure, soil moisture conditions, land-use intensity, and surface sealing, all of which influence infiltration, evapotranspiration, and runoff generation. Vegetated

surfaces with dense canopy cover typically exhibit greater interception and infiltration capacity, while impervious urban surfaces generate rapid runoff and heightened flood potential. Quantitative flood studies have demonstrated that spectral indices derived from multispectral imagery correlate with flood occurrence probability, particularly when analyzed across seasonal and climatic gradients (Gigović et al., 2017).

Figure 2: LiDAR Technology for High-Resolution Terrain Mapping

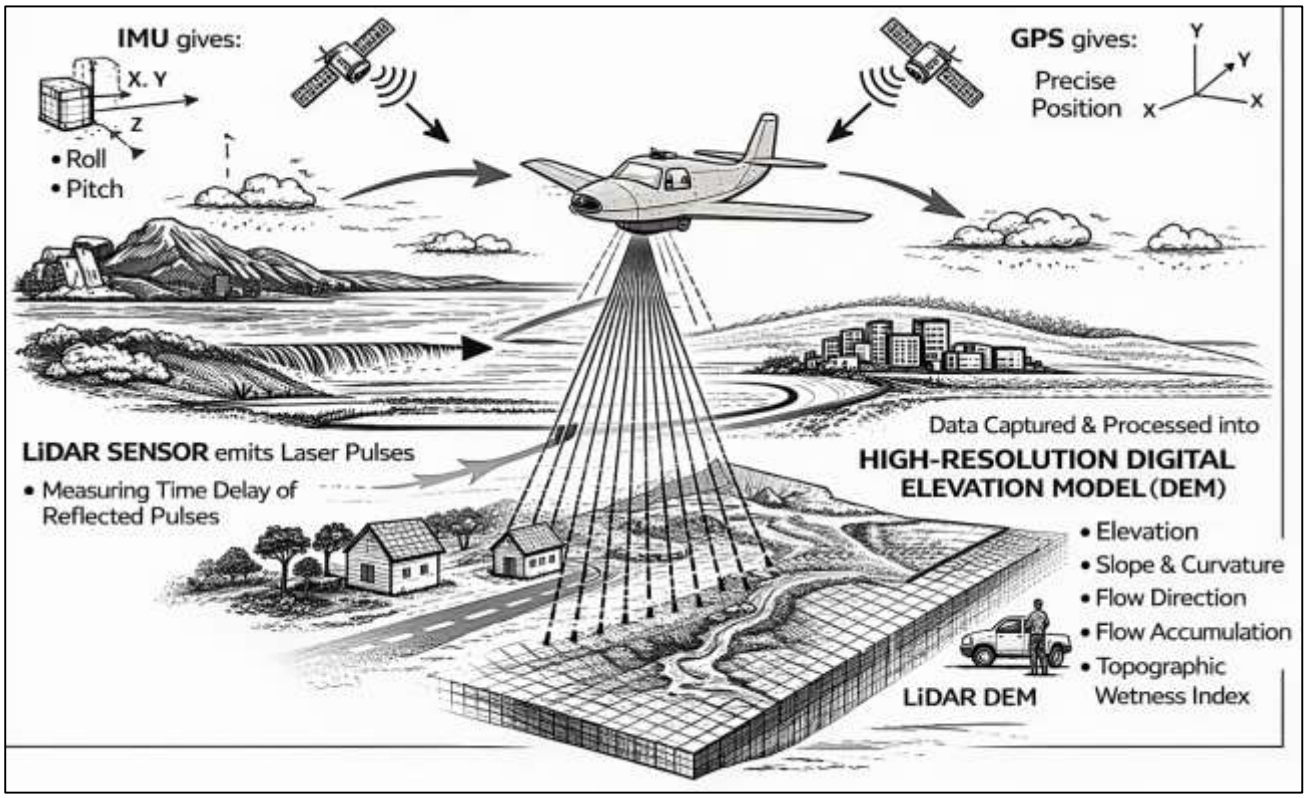

Temporal sequences of multispectral observations further enable detection of land-cover change, agricultural cycles, and urban expansion, which modify flood vulnerability over time. In riverine and coastal contexts, multispectral data support delineation of wetlands, floodplains, and sediment deposition zones that mediate flood attenuation. International research efforts have shown that multispectral features enhance flood hazard prediction when combined with terrain-based indicators, as they capture surface conditions that terrain alone cannot represent. However, spectral signals are subject to atmospheric interference, illumination variability, and sensor-specific noise, introducing uncertainty into quantitative models (Wang et al., 2015). These challenges highlight the need for analytical frameworks that can learn robust feature representations from noisy multispectral inputs. When integrated with elevation data, multispectral signatures provide a more complete depiction of the land surface as a coupled physical and biological system. This integration aligns with contemporary hydrological theory, which views flooding as an emergent outcome of interactions among terrain, surface cover, and meteorological forcing rather than a function of elevation alone.

Deep learning represents a class of machine learning methods characterized by hierarchical feature learning through multi-layer neural architectures (Toosi et al., 2019). In geospatial analytics, deep learning has gained prominence due to its capacity to model complex, non-linear relationships in high-dimensional data. Unlike traditional statistical approaches that rely on predefined feature interactions, deep learning models learn representations directly from data, enabling them to capture subtle spatial patterns and contextual dependencies. Convolutional neural networks (CNNs) have been particularly influential in remote sensing applications because of their ability to exploit spatial structure and neighborhood information inherent in raster data. Quantitative flood mapping studies employing deep learning have reported improvements in classification accuracy, spatial coherence, and generalization

across regions. These models have been applied to tasks including flood extent delineation, susceptibility mapping, and damage assessment (Jinnat & Kamrul, 2021; Nandi et al., 2016). From a methodological standpoint, deep learning is well suited to data fusion problems, as it can integrate heterogeneous inputs such as elevation grids and multispectral imagery within unified architectures. International research has demonstrated that deep models can learn joint representations that preserve the complementary strengths of different sensing modalities (Zulqarnain & Subrato, 2021). However, deep learning introduces challenges related to interpretability, data requirements, and computational complexity. In flood hazard research, these challenges are addressed through careful model design, validation strategies, and feature attribution analyses. The adoption of deep learning reflects a broader shift toward viewing flood vulnerability as a spatial learning problem rather than a purely physical simulation task (Kundzewicz et al., 2017; Akbar & Sharmin, 2022). This shift aligns with the increasing availability of large-scale geospatial datasets and the need for scalable, transferable modeling solutions. Data fusion refers to the systematic integration of information from multiple sources to produce representations that are more informative than those derived from individual datasets. In flood hazard mapping, fusion of LiDAR-derived terrain features and multispectral surface signatures enables simultaneous modeling of structural and functional land-surface properties. Quantitative studies have shown that fused datasets outperform single-source inputs in predicting flood susceptibility, as they capture interactions between elevation-driven flow dynamics and surface-mediated runoff processes (Manfreda et al., 2015; Foysal & Subrato, 2022). Fusion can occur at multiple levels, including feature-level concatenation, representation-level integration, and decision-level aggregation. Deep learning architectures facilitate representation-level fusion by learning shared latent spaces that encode cross-modal relationships. International flood research increasingly adopts fusion-based approaches to address the limitations of individual data modalities. For example, terrain models may identify low-lying areas, while multispectral data distinguish permeable floodplains from impervious urban basins within those areas. The combined representation enhances discrimination between zones with similar elevation but different hydrological behavior (Baky et al., 2020; Zulqarnain, 2022). Quantitative validation across diverse landscapes has demonstrated that fusion-based models exhibit greater robustness to regional variability and land-cover heterogeneity. These findings underscore the value of integrating physical and spectral information within unified predictive frameworks. Fusion-based flood hazard modeling aligns with interdisciplinary perspectives that emphasize the coupled nature of earth surface processes. By leveraging complementary data sources, such models provide a more nuanced characterization of land-surface vulnerability that is responsive to both morphology and composition (Abdul, 2023; Gori et al., 2020; Hammad & Mohiul, 2023).

Contemporary flood hazard mapping extends beyond binary classification of flooded versus non-flooded areas toward probabilistic and ranking-based representations of risk. In operational contexts, decision-makers require spatial prioritization of vulnerable zones to allocate resources, design mitigation measures, and plan emergency response (Hasan & Waladur, 2023; Rifat & Rebeka, 2023). Quantitative flood models therefore emphasize discrimination and calibration rather than absolute prediction. Risk scores generated by deep learning models are interpreted as relative measures of vulnerability, enabling comparison across locations and scales. International disaster management frameworks increasingly adopt risk-based approaches that integrate hazard probability with exposure and vulnerability metrics (Demir & Kisi, 2016; Masud & Hossain, 2024; Zulqarnain & Subrato, 2023). Within this framework, land-surface vulnerability prediction supports proactive planning by identifying areas where flooding would produce disproportionate impacts. The integration of LiDAR and multispectral data within deep learning models enhances the reliability of these risk rankings by grounding them in both terrain structure and surface condition. Empirical evaluations have shown that top-ranked vulnerability zones often account for a large share of observed flood damage, reinforcing the value of prioritization over exhaustive prediction (Antzoulatos et al., 2022; Md & Sai Praveen, 2024; Nahid & Bhuya, 2024). This perspective situates flood hazard mapping within a broader paradigm of quantitative risk analytics, where models are evaluated based on their ability to support actionable decision-making under uncertainty. The framing of flood vulnerability as a continuous spatial phenomenon aligns with international efforts to shift from reactive disaster response toward anticipatory risk management grounded in data-driven evidence (Bathrellos et al., 2016; Newaz &

Jahidul, 2024; Akbar, 2024).

The objective of this quantitative study is to develop and validate a deep learning–enabled modeling framework that fuses LiDAR-derived topographic information with multispectral reflectance signatures to improve flood hazard mapping and land-surface vulnerability prediction across heterogeneous landscapes. The study operationalizes flood hazard and vulnerability as measurable spatial outcomes that can be estimated from engineered and learned representations of terrain morphology, hydrologic connectivity, land-cover composition, and surface condition indicators derived from remote sensing sources. A central objective is to quantify the incremental value of multimodal data fusion by systematically comparing model performance under LiDAR-only, multispectral-only, and combined-input configurations, using consistent validation protocols and identical evaluation targets. The study also aims to assess how different fusion strategies influence predictive discrimination and ranking utility, treating the output as a continuous risk surface that supports prioritization of high-vulnerability zones rather than as a purely binary classification product. To ensure that the results reflect realistic deployment conditions, an additional objective is to evaluate model generalization under spatial and contextual heterogeneity by testing performance across corridor-like geographic partitions, land-cover regimes, and terrain classes, thereby measuring robustness to changes in physiographic setting and surface structure. The study further targets calibration quality by examining whether predicted vulnerability scores correspond to observed flood occurrence frequencies and whether score distributions yield stable thresholds for operational mapping and planning use. Another objective is to examine the sensitivity of the framework to data resolution and feature scaling, particularly in the integration of fine-resolution LiDAR derivatives with multispectral inputs that may vary in spatial granularity and atmospheric noise characteristics. Finally, the study seeks to establish a reproducible model-development workflow that includes standardized preprocessing, feature harmonization, and controlled training routines, enabling transparent model validation and audit-ready reporting of performance. Collectively, these objectives position the research as a model-development and model-validation investigation designed to produce empirically verifiable evidence on the extent to which deep learning–based LiDAR–multispectral fusion improves flood hazard characterization and land-surface vulnerability ranking under quantitative evaluation criteria.

LITERATURE REVIEW

This Literature Review consolidates quantitative scholarship relevant to Deep Learning–Enabled LiDAR and Multispectral Signature Fusion for Flood Hazard Mapping and Land-Surface Vulnerability Prediction by organizing prior work around measurable variables, modeling assumptions, and validation practices used in flood susceptibility and inundation risk research (Kazakis et al., 2015). The section is structured to connect four evidence streams that directly shape quantitative model development: (1) hydrologic and geomorphologic determinants of flood hazard that can be operationalized as predictors, (2) LiDAR-based terrain representation and derivative feature engineering for flood modeling, (3) multispectral reflectance signatures and land-surface descriptors that capture surface permeability, vegetation structure, and built-up intensity, and (4) deep learning architectures and fusion strategies designed to combine heterogeneous geospatial modalities into unified predictive representations. Emphasis is placed on how studies define flood hazard and vulnerability as supervised targets or proxy outcomes, how they treat class imbalance and rare-event behavior, and how they evaluate model utility using discrimination, calibration, and ranking-based metrics aligned with decision workflows (Emerton et al., 2017). The review also synthesizes comparative evidence on baseline statistical methods versus ensemble and neural approaches, focusing on what is gained quantitatively when moving from hand-engineered indicators to representation learning. The goal of this section is to establish a measurement-driven foundation for the present study's modeling choices by identifying which predictors, fusion mechanisms, and validation designs have produced consistent performance gains under realistic geographic heterogeneity and data-quality constraints.

Framing for Flood Hazard and Land-Surface Vulnerability

The quantitative flood-risk literature increasingly defines flood hazard as a spatially continuous probability surface rather than a binary event indicator. Early flood mapping approaches relied on categorical representations in which locations were labeled as flooded or non-flooded based on observed inundation boundaries or historical records. While operationally simple, binary labeling compresses substantial variability in flood intensity, duration, and frequency into a single outcome class. More recent studies conceptualize flood hazard as a probabilistic phenomenon, expressing risk as a continuous measure that reflects the likelihood or severity of inundation conditioned on terrain, hydrologic connectivity, and surface characteristics. This framing aligns with broader risk science paradigms that treat hazards as gradients rather than discrete states (Akay, 2021).

Figure 3: Flood Hazard and Vulnerability Framework

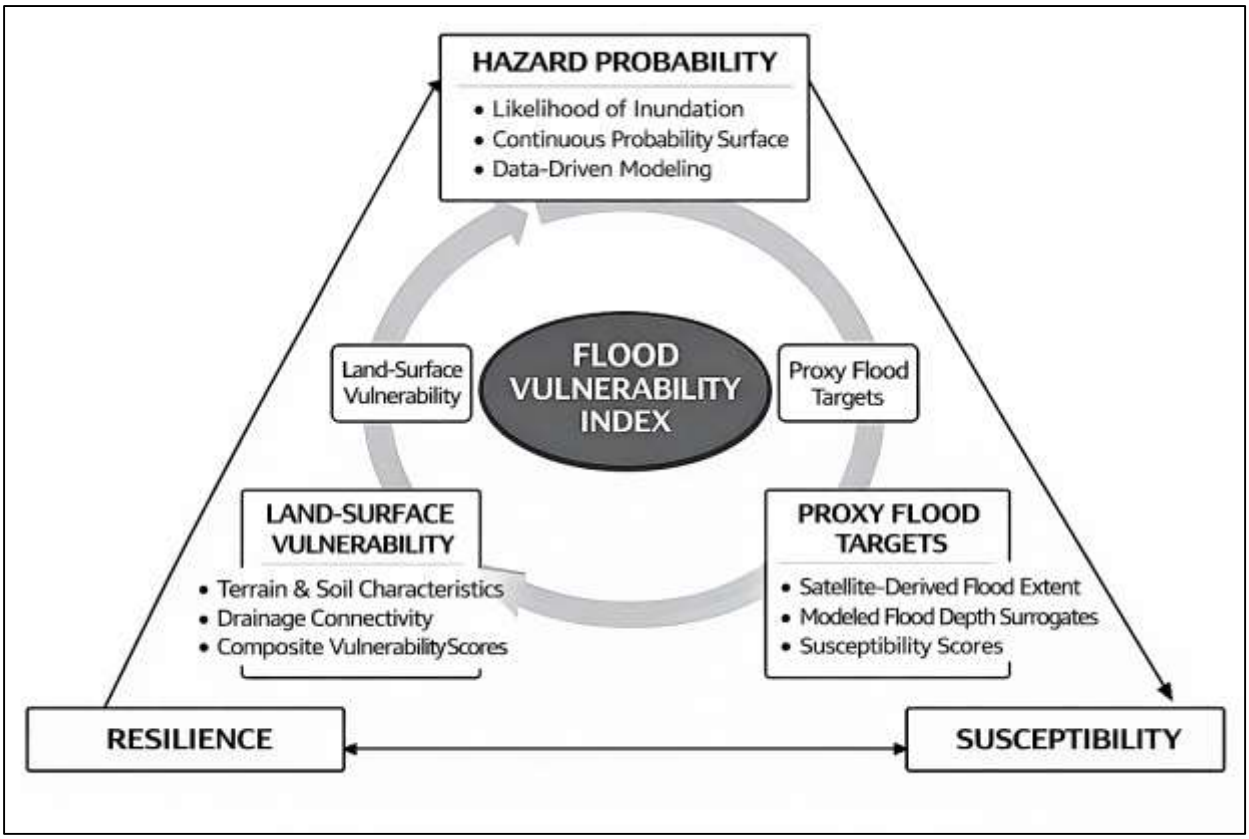

Quantitative research demonstrates that continuous hazard indices preserve ranking information that is lost in threshold-based classification, enabling prioritization of high-risk zones even when absolute flood occurrence is uncertain. Probability surfaces also support calibration analysis, allowing predicted scores to be compared with observed event frequencies across spatial strata. In data-driven flood modeling, probability-based outputs facilitate evaluation under class imbalance, where flooded observations represent a small fraction of the spatial domain (Kumar & Acharya, 2016). The literature further indicates that probabilistic representations are more robust to label noise arising from incomplete flood detection or sensor limitations, since uncertainty can be absorbed into score distributions rather than forcing hard class assignments. These characteristics have led to widespread adoption of continuous hazard scores in machine learning–based flood susceptibility studies, particularly when outputs are intended to support spatial planning and comparative risk assessment across large geographic regions.

Land-surface vulnerability is treated in the literature as an emergent property arising from the interaction of terrain morphology, surface composition, and hydrological connectivity rather than as a single observable variable. Quantitative studies consistently operationalize vulnerability using composite representations that integrate elevation, slope, curvature, land-cover type, soil characteristics, and proximity to drainage networks (Papaioannou et al., 2015). This multidimensional

framing reflects hydrological theory, which emphasizes that flood response is governed jointly by gravitational flow paths, infiltration capacity, surface roughness, and storage potential. Terrain variables determine the direction and concentration of surface runoff, while land-cover attributes regulate permeability, interception, and evapotranspiration. Drainage connectivity metrics capture how efficiently excess water is conveyed toward channels or depressions. Empirical evidence shows that none of these components alone provides sufficient explanatory power for flood susceptibility, particularly across heterogeneous landscapes that include urban, agricultural, and natural surfaces. Composite vulnerability indicators enable normalization across physiographic contexts, allowing similar risk interpretations in areas with different absolute elevations or rainfall regimes (Uddin & Matin, 2021). The literature also emphasizes that vulnerability is spatially structured, exhibiting autocorrelation and scale dependency, which necessitates modeling approaches that preserve neighborhood relationships. This has motivated the use of raster-based representations where vulnerability emerges from local spatial context rather than isolated pixel attributes. By treating vulnerability as a composite spatial construct, quantitative flood studies align measurement frameworks with the physical processes governing surface-water dynamics and support integrative modeling strategies that can accommodate diverse environmental settings (Lyu et al., 2016).

Because direct observations of flood processes are often incomplete or unavailable, flood hazard research relies heavily on proxy targets that approximate inundation and vulnerability outcomes. The literature describes several classes of proxy targets, including flood extent masks derived from satellite imagery, depth surrogates inferred from hydrodynamic models, and susceptibility scores generated from expert-based weighting schemes. Flood extent masks are commonly extracted from optical or radar imagery and serve as binary or probabilistic indicators of observed inundation during specific events. While valuable, these masks are temporally constrained and may omit short-duration or obscured flooding (Erena et al., 2018; Rabiul & Alam, 2024; Sai Praveen, 2024). Depth surrogates provide continuous targets that capture intensity but depend on modeling assumptions and boundary conditions that introduce uncertainty. Susceptibility scores, constructed through multi-criteria decision analysis or statistical aggregation, represent relative vulnerability rather than direct physical outcomes. Quantitative studies highlight that each proxy type embodies trade-offs between realism, coverage, and noise. Consequently, model evaluation must account for the limitations of target construction rather than treating labels as error-free ground truth (Hammad & Hossain, 2025; Liu et al., 2016; Azam & Amin, 2024). The literature further notes that proxy targets influence apparent model performance, as smoother susceptibility indices may yield higher discrimination metrics than noisy event-based labels. Robust flood modeling therefore emphasizes consistency between predictor variables and target definitions, ensuring that learned relationships reflect meaningful hydrological patterns rather than artifacts of label construction (Cao et al., 2016).

The choice of unit of analysis plays a critical role in flood hazard modeling and directly influences how vulnerability and uncertainty are represented. Pixel-level modeling is widely used due to its compatibility with raster remote sensing data and its ability to capture fine-scale spatial variation. However, pixel-based approaches may amplify noise arising from mixed land-cover signals and sensor resolution limits. Object- or polygon-based units, such as hydrological response units or administrative parcels, aggregate information to reduce variability but risk obscuring localized flood pathways (Mosheur, 2025; Thapa et al., 2020). Grid aggregation offers a compromise by standardizing spatial units while preserving spatial continuity. The literature emphasizes that unit selection should align with both data resolution and decision context. Label error is closely intertwined with unit choice, as temporal misalignment between flood events and satellite acquisitions can lead to false negatives, while cloud contamination and mixed pixels introduce classification ambiguity. These errors propagate differently depending on spatial aggregation, affecting both model training and evaluation. Quantitative studies increasingly address label uncertainty through probabilistic modeling and validation designs that recognize imperfect observation. Rather than eliminating error, contemporary approaches seek to manage it through robust evaluation and sensitivity analysis (Abdelkarim et al., 2020). This perspective positions flood hazard modeling as an inference problem under uncertainty, where measurement framing is as influential as algorithmic choice.

Hydrologic Used in Flood Susceptibility Modeling

Beyond elevation, slope and curvature are frequently treated as core geomorphic predictors because they characterize the mechanics of runoff generation and convergence across landscapes. Slope is used to represent the potential speed of overland flow and the likelihood that rainfall becomes rapid surface runoff rather than infiltrating or being stored locally (Orton et al., 2016). In many quantitative models, flatter slopes are associated with higher inundation susceptibility because low-gradient surfaces tend to promote water retention and lateral spreading, especially when drainage pathways are capacity-limited. Curvature variables add important nuance by distinguishing between convex surfaces that tend to shed water and concave forms that tend to collect and concentrate flow.

Figure 4: Terrain-Based Flood Susceptibility Framework

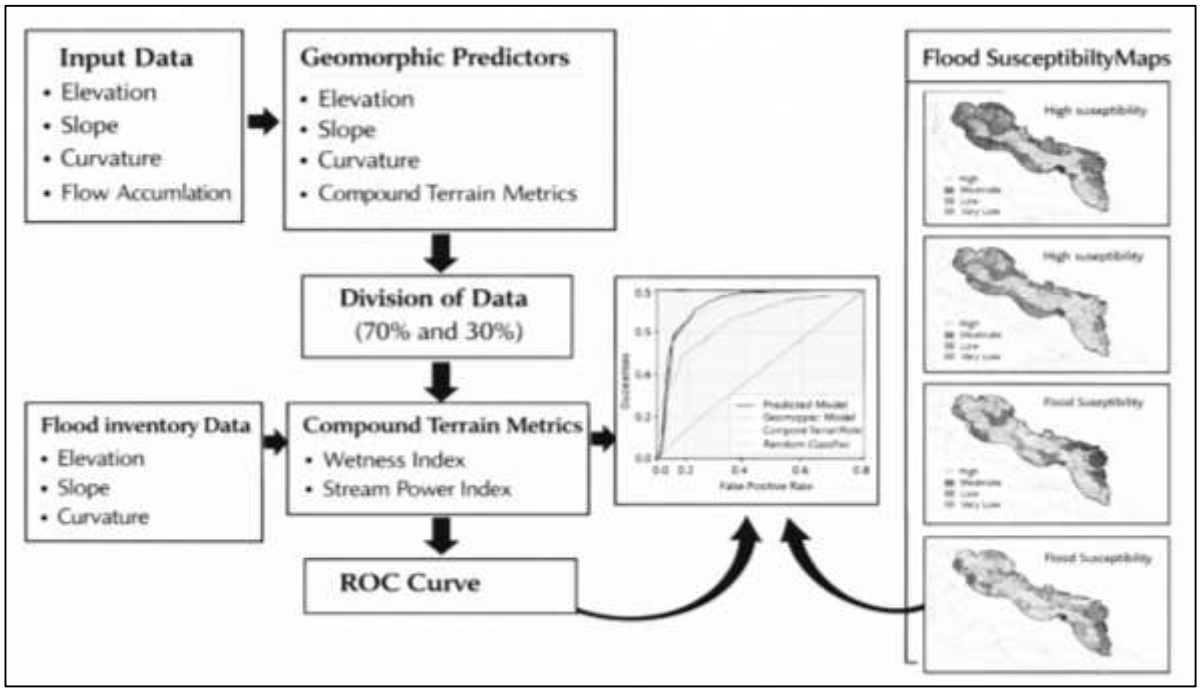

This distinction becomes particularly relevant in valley bottoms, small basins, and anthropogenically modified terrain where localized concavities function as pooling zones. Flow accumulation is widely used as a proxy for how much upstream contributing area feeds a location, allowing models to encode network-like hydrologic convergence even when channel data are incomplete (De Moel et al., 2015). The literature underscores that these variables are most informative when evaluated together, because a cell with large contributing area and concave curvature on a low slope forms a consistent hydrologic signature of flood-prone settings. At the same time, susceptibility studies note that slope, curvature, and accumulation are sensitive to DEM preprocessing choices such as sink filling, breaching, and resolution, which can alter derived surfaces and change apparent risk gradients. For this reason, many quantitative studies treat these predictors as scale-dependent indicators whose effects are validated across multiple resolutions or landscape partitions to verify stability and interpretability under differing terrain regimes (Zaharia et al., 2017).

A large portion of flood susceptibility literature incorporates compound terrain metrics that combine multiple geomorphic elements into single indicators intended to approximate hydrologic processes. Common examples include wetness-related measures that represent potential soil saturation and storage, and energy-related measures that capture erosive or transport potential in concentrated flows. These compound metrics are valued because they translate elevation structure into process-oriented signals that better align with runoff behavior under rainfall events (Saharia et al., 2017). In susceptibility models, wetness-oriented indicators are often interpreted as spatial proxies for where water is likely to persist because of contributing area and low-gradient conditions, thereby linking terrain form to moisture retention and ponding. Energy-related indicators are used to represent where concentrated

flow may form preferential pathways, particularly in steeper catchments or incised valleys where runoff concentrates quickly (Schubert et al., 2017). The literature describes compound metrics as especially helpful in bridging purely geometric terrain representation with hydrologic plausibility, providing variables that can improve discrimination when used alongside basic predictors such as elevation and slope. However, studies also caution that compound metrics remain indirect proxies and are sensitive to DEM artifacts, drainage enforcement, and the scale at which contributing area is computed. As a result, many quantitative flood studies evaluate these indicators through comparative modeling or feature contribution analysis, examining whether compound variables improve classification or ranking performance relative to simpler geomorphic predictors (Moftakhari et al., 2017). This line of work positions compound terrain metrics as intermediate representations that operationalize hydrologic logic in data-driven susceptibility modeling

LiDAR-Enabled Terrain Representation for Flood Hazard Mapping

The flood hazard mapping literature consistently treats LiDAR-derived elevation products as a methodological turning point because they capture fine-scale topographic variation that governs inundation pathways, ponding, and floodplain connectivity. LiDAR-based DEM/DTM construction is generally described as a measurement process in which point-cloud returns must be filtered into ground and non-ground classes, interpolated into continuous surfaces, and validated against control points or surveyed benchmarks (Hazarika et al., 2018).

Figure 5: LiDAR-Driven Flood Hazard Mapping

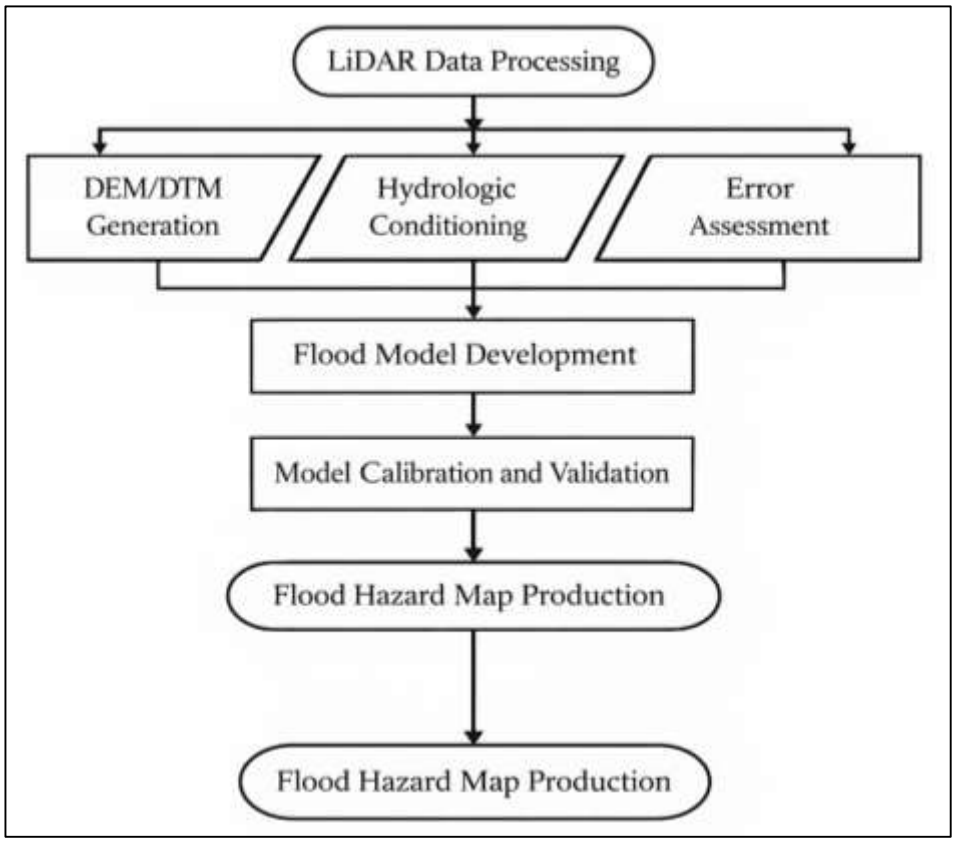

Studies emphasize that the value of LiDAR for flood applications is strongly tied to vertical accuracy, because small elevation biases can materially shift predicted flood extent and apparent exposure, particularly in low-relief floodplains, coastal zones, and urban basins where centimeter-to-decimeter differences determine flow direction and storage. In quantitative terms, vertical errors propagate into flood models through slope and flow-routing derivations, drainage boundary placement, and the delineation of micro-barriers such as levees, road crowns, and embankments. The literature also highlights that error is not uniform across land covers; vegetation, water surfaces, and complex urban geometry can introduce spatially structured inaccuracies through misclassification, reduced ground

returns, and interpolation artifacts (Oulahen et al., 2015). These uncertainties are often framed as consequential for both deterministic hydraulic mapping and data-driven susceptibility modeling, where the same elevation surface is used to derive predictors such as relative elevation, curvature, and flow accumulation. Researchers therefore treat LiDAR quality assessment as inseparable from flood modeling validity, describing practices such as reporting vertical error summaries, inspecting terrain artifacts, and evaluating how uncertainty influences mapped hazard zones and risk ranks in downstream analytics (Arnell & Gosling, 2016).

A major theme in LiDAR-enabled flood research is that raw elevation surfaces are rarely hydrologically "ready" for modeling, because measurement noise and sampling gaps produce artificial pits, spurious dams, and disconnected channels that distort flow simulation and derived terrain predictors. Hydrologic conditioning is therefore treated as a standard preprocessing stage that aims to enforce physically plausible drainage connectivity. Sink filling is widely discussed as a method for removing small depressions that arise from interpolation noise or vegetation artifacts, enabling continuous flow paths in raster routing (Santos et al., 2020). Breaching procedures are described as an alternative that cuts through artificial barriers rather than raising depressions, which is often considered more realistic in landscapes where roads, levees, and embankments can be overrepresented by rasterization and cause flow blocking. Channel enforcement practices, including carving known river centerlines or incorporating surveyed bathymetry proxies when available, are emphasized because flood behavior depends heavily on channel conveyance geometry that is not always captured by airborne LiDAR, especially when water surfaces limit returns or when channels are narrow relative to grid resolution. The literature also notes that conditioning choices influence model outcomes in systematic ways: aggressive sink filling can eliminate true hydrologic storage features such as wetlands or shallow basins, while insufficient conditioning preserves artifacts that misroute flow and inflate the apparent role of topographic barriers (Woodrow et al., 2016). For susceptibility modeling, these effects translate into altered distributions of flow accumulation, wetness-related indicators, and drainage proximity measures, changing which areas are learned as high-risk. As a result, many studies treat conditioning as a sensitivity factor and document conditioning settings as part of reproducible flood hazard workflows (Wu et al., 2024).

Multispectral Signature Features of Surface Runoff Potential

The flood susceptibility and hydrologic remote sensing literature frequently treats multispectral reflectance as an indirect yet powerful descriptor of surface conditions that regulate runoff generation and water retention. The basic premise is that surface reflectance patterns encode land-cover composition, vegetation density, soil exposure, and moisture-related properties that correlate with infiltration capacity and surface sealing (Petrasova et al., 2017). In quantitative mapping studies, these spectral signals are operationalized as permeability proxies because impervious or compacted surfaces tend to generate faster runoff and higher ponding potential, while vegetated or porous surfaces tend to support infiltration and interception. Land-cover classification derived from multispectral imagery is therefore often positioned as a foundational input in flood vulnerability modeling, particularly in mixed land-use basins where hydrologic response varies sharply across short distances. Studies also emphasize that surface condition matters alongside land cover, since agricultural stages, soil disturbance, and vegetation stress can modify runoff behavior even within the same nominal class (O'Neil et al., 2019). This leads to modeling practices that incorporate both categorical land-cover labels and continuous spectral descriptors, allowing vulnerability to be expressed as a gradient of surface response rather than a binary distinction. In urban and peri-urban settings, multispectral features are commonly interpreted as indicators of built-up intensity, thermal and material composition, and surface roughness proxies that relate to drainage behavior. Across this literature, multispectral reflectance is treated not as a direct measurement of hydrologic flow but as a quantitative representation of surface states that influence rainfall partitioning into infiltration, storage, and runoff pathways (Rocha et al., 2022).

A consistent methodological stream in flood hazard research uses spectral indices as compact predictors that translate multispectral bands into interpretable environmental indicators relevant to vulnerability. Vegetation-related indices are widely used to represent canopy density and plant vigor, which are associated with interception and infiltration behavior (Prior et al., 2024). Water-related

indices are frequently used to delineate open water and saturated surfaces, providing direct mapping of water bodies and indirect signals of wetness-prone zones. Built-up indices are commonly applied to identify impervious surfaces and urban expansion, which increase runoff speed and reduce infiltration. Bare soil indices serve as proxies for exposed ground conditions that influence runoff depending on compaction, texture, and disturbance. The literature highlights that these indices are attractive in quantitative modeling because they provide standardized, sensor-compatible measures that reduce dimensional complexity while preserving physically meaningful interpretation (Mihu-Pintilie et al., 2019).

Figure 6: Spectral Indices in Flood Vulnerability

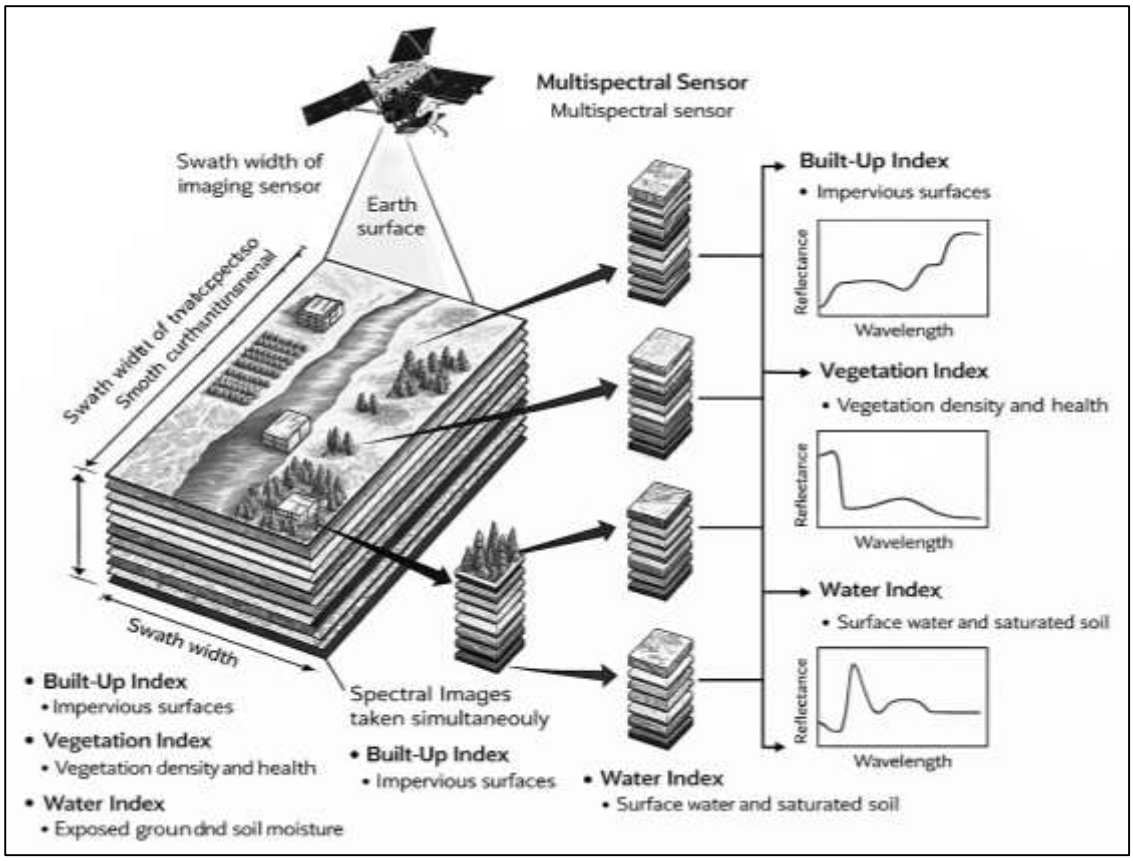

Many studies incorporate multiple indices simultaneously to capture interactions between vegetation cover, moisture signatures, and built-up intensity, supporting more nuanced discrimination of vulnerable zones. At the same time, research cautions that index behavior is context sensitive, shifting with atmospheric conditions, sensor characteristics, seasonal phenology, and soil background effects. Consequently, index-based predictors are frequently paired with normalization procedures, land-cover stratification, or temporal compositing to stabilize signals for predictive modeling. In flood mapping workflows, index features are often validated through sensitivity analysis and comparative modeling to determine whether they improve discrimination relative to raw spectral bands or categorical land-cover products, positioning indices as intermediate representations that bridge multispectral measurement and hydrologic interpretation (Lindsay et al., 2019).

Flood vulnerability studies repeatedly emphasize that multispectral predictors are temporally variable, meaning that a single-date image can reflect seasonal phenology, agricultural cycles, and short-term moisture anomalies that confound stable susceptibility estimation. Vegetation indices change across growing seasons, rainfall regimes, and cropping calendars, while soil and surface moisture signatures can shift rapidly after storms (Pinel et al., 2015). This variability introduces measurement instability when models are trained on imagery captured at different dates, making temporal alignment a major concern in quantitative flood analytics. Temporal compositing is widely discussed as a strategy to stabilize multispectral predictors by aggregating observations across defined periods, selecting representative values, or filtering out contaminated scenes. Researchers describe compositing as

beneficial for reducing noise caused by clouds, haze, and variable illumination, while also providing seasonally representative surface states (Boulton & Stokes, 2018). In addition, multi-temporal feature construction is frequently used to represent land-surface dynamics, such as seasonal greenness patterns, persistent wetness behavior, or recurring bare-soil exposure, all of which relate to runoff potential and drainage response. Studies also note that the choice of temporal window affects the meaning of predictors: short windows may retain event sensitivity, while longer windows emphasize baseline vulnerability. The literature frames these choices as measurement decisions that must be justified in relation to the modeling target, whether that target is event-specific inundation mapping or longer-term vulnerability prediction. Through this lens, seasonality and compositing are treated as integral components of predictor design rather than secondary preprocessing steps (Bernard et al., 2022).

Quantitative flood vulnerability research consistently identifies urbanization and imperviousness as major drivers of runoff concentration and ponding, and multispectral imagery is widely used to detect built-up intensity at scale. Spectral–spatial metrics that combine index behavior with texture or neighborhood patterns are frequently applied to differentiate dense built cores, mixed residential zones, industrial surfaces, and peri-urban expansion areas where drainage capacity is often mismatched to surface sealing. The literature highlights that urban detection is not purely a classification task; rather, it functions as a quantitative estimation of runoff-producing surface proportion, which directly affects susceptibility modeling (Wong et al., 2021). This makes radiometric normalization and atmospheric correction especially important, because urban materials and bare soil can exhibit similar spectral responses under variable illumination or aerosol conditions. Research repeatedly shows that inadequate correction can shift reflectance distributions, alter index values, and create non-comparable predictors across scenes, which can distort coefficients in statistical models or learned feature embeddings in neural models. To address this, studies employ standardized atmospheric correction workflows and cross-scene normalization strategies to stabilize multispectral inputs for modeling (Grau et al., 2021). The literature also discusses that sensor differences and bandpass variability can influence derived predictors, motivating harmonization when multi-sensor datasets are used. In flood mapping contexts where small differences in predicted vulnerability can influence spatial prioritization, these radiometric considerations are treated as directly relevant to model validity and reproducibility. Overall, multispectral-based urban imperviousness estimation and radiometrically disciplined preprocessing are positioned as key conditions for producing reliable flood vulnerability predictors that generalize across space and acquisition periods (Rocha et al., 2020).

Data Fusion Strategies for LiDAR

Quantitative flood modeling studies frequently describe feature-level fusion as the most direct strategy for combining LiDAR-derived terrain variables and multispectral surface descriptors, because it converts both modalities into a single predictor table that can be ingested by statistical learners, tree ensembles, or neural networks. In this approach, engineered LiDAR derivatives (elevation, relative height, slope, curvature, flow-related surfaces, roughness measures) are concatenated with multispectral bands and indices that represent vegetation condition, built-up intensity, bare soil exposure, and water-related signals (Nguyen et al., 2016). The literature highlights that feature-level fusion supports transparent variable accounting, enabling investigators to trace model sensitivity back to specific predictors and to compare the added value of each feature family. At the same time, researchers emphasize that concatenation introduces multicollinearity and redundancy because many LiDAR derivatives are mathematically related, and multispectral indices often share overlapping spectral information. This collinearity can destabilize coefficient-based models and complicate interpretability, particularly when predictors cluster strongly by terrain scale or land-cover regime. Consequently, studies commonly apply feature screening, correlation filtering, variance-based reduction, or regularized estimation to stabilize fused models while preserving discriminative content (Pearson et al., 2023). Another recurring theme is that feature-level fusion is sensitive to scaling and normalization choices, because LiDAR variables and spectral predictors occupy different numeric ranges and distribution shapes. In flood susceptibility settings with class imbalance, fusion models are also evaluated for ranking utility, since the operational goal often involves prioritizing the highest-risk zones rather than optimizing overall accuracy. Within this literature, feature-level fusion is treated as

a baseline fusion paradigm that provides measurable gains when redundancies are controlled and predictors are harmonized under consistent preprocessing routines (Dietrich & Krautblatter, 2019). Representation-level fusion is discussed in the geospatial machine learning literature as a method that integrates LiDAR and multispectral inputs earlier in the modeling pipeline by learning shared latent representations rather than simply concatenating handcrafted predictors. In flood mapping studies, this strategy is commonly described through dual-stream designs in which one encoder processes elevation-derived rasters and the other processes multispectral imagery, followed by a fusion stage that combines intermediate feature maps or embeddings (Rallapalli et al., 2022).

Figure 7: Data Fusion Approach to Flood Risk

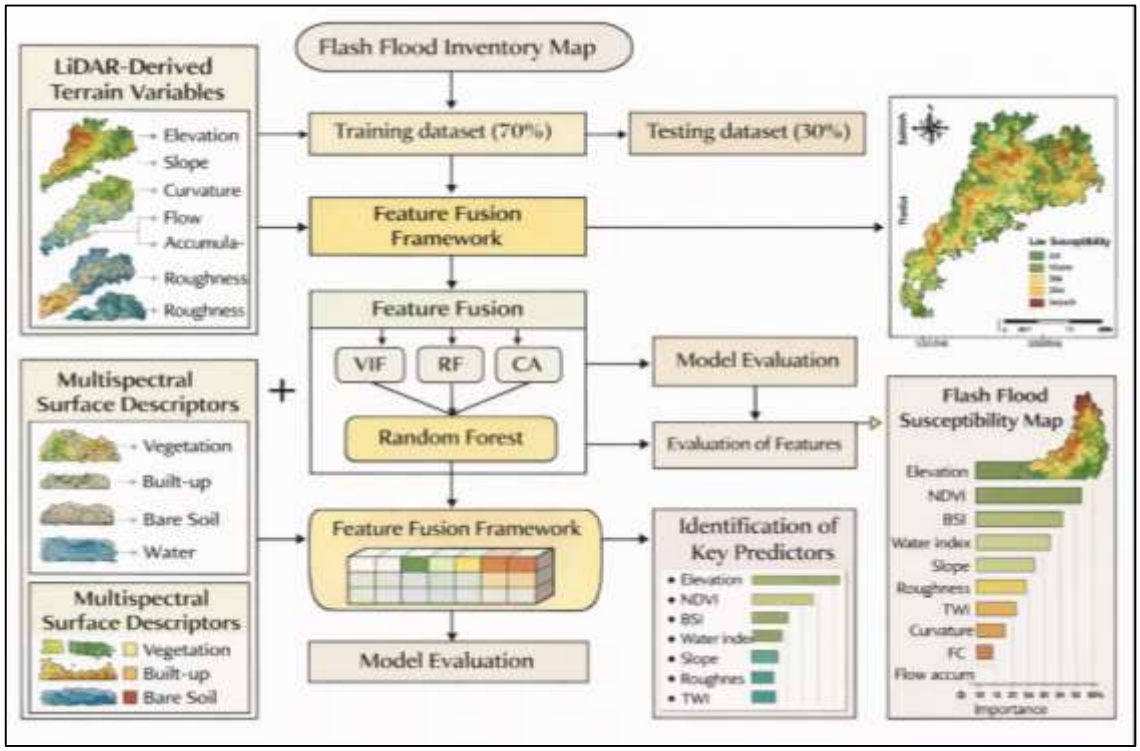

The motivation emphasized across studies is that LiDAR and multispectral data encode different "views" of the same landscape—structural geometry versus surface composition—and these views interact in non-linear ways that are difficult to capture through manual feature engineering alone. Representation-level fusion frameworks allow models to learn cross-modal correspondences, such as identifying that low-lying depressions become more flood-prone when paired with impervious spectral signatures or when vegetation indicators suggest limited infiltration. The literature also treats this approach as well-suited to spatial pattern learning, because convolutional encoders can incorporate neighborhood context, capturing localized drainage controls and urban micro-basins that influence flood accumulation (Chen et al., 2018). A recurring methodological issue concerns alignment: when LiDAR and multispectral rasters differ in resolution, projection, or acquisition timing, the learned embedding may reflect misregistration artifacts rather than hydrologic structure. Researchers therefore emphasize careful co-registration, resampling discipline, and patch design so that encoders receive spatially coherent inputs. In evaluation, representation-level fusion is often interpreted through ranking performance and spatial consistency of predicted surfaces, since fused embeddings can produce smoother and more hydrologically plausible risk gradients than models trained on single modalities. Overall, the literature frames representation-level fusion as a mechanism for capturing interaction-heavy vulnerability patterns embedded in joint terrain–surface conditions (Lay et al., 2019). Decision-level fusion is widely presented as a practical alternative when LiDAR and multispectral modalities differ in coverage, resolution, or reliability across a study region. Instead of forcing early fusion, researchers train separate models—one based on LiDAR-only predictors and another based on multispectral-only predictors—and combine their outputs through averaging, weighted voting, or

stacked generalization. The literature positions stacked ensembles as especially useful in flood risk mapping because different models can specialize in different error regimes: LiDAR-based models may excel at detecting low-relief basins and drainage corridors, while spectral models may better capture imperviousness gradients, vegetation-mediated infiltration differences, and land-cover heterogeneity (Saleem et al., 2019). Decision-level fusion also supports modular validation, allowing investigators to quantify each model's independent value before evaluating combined performance. This separation is treated as beneficial under label uncertainty, since disagreement between models can highlight ambiguous zones where mapping confidence is lower. In some quantitative studies, stacked fusion is described as reducing variance and stabilizing performance across spatial partitions, particularly when the study area includes multiple terrain classes or mixed urban–rural configurations. A common evaluation emphasis is top-ranked alert quality, where the combined model is judged by its ability to correctly identify the highest-risk subset of locations or grid cells (Saleem et al., 2019). Decision-level fusion is also frequently discussed as interpretability-friendly, since component models can be inspected separately and their contributions to the final risk score can be summarized through weights or meta-learner feature importance. Within the broader remote sensing and hazard analytics literature, decision fusion is treated as a robust integration method that can deliver consistent improvements when modalities provide complementary error reductions rather than redundant signals (Rong et al., 2020).

Studies on LiDAR–multispectral flood modeling repeatedly emphasize that fusion performance depends on spatial resolution harmonization, because LiDAR elevation products often provide finer grid spacing than multispectral imagery. Upsampling coarser spectral rasters to match LiDAR resolution can create interpolated artifacts that exaggerate spatial detail without adding information, while downsampling LiDAR can smooth microtopography and remove small barriers and depressions that influence flood pathways (Dey et al., 2019). The literature treats these resampling choices as measurement interventions that can materially affect discrimination, calibration, and ranking behavior in flood susceptibility outputs. Researchers therefore examine resolution sensitivity through controlled experiments that compare models trained at multiple resolutions, evaluating whether improvements are stable or driven by scale-specific artifacts. Another prominent practice is fusion ablation, where model configurations are systematically reduced to isolate the marginal contribution of each modality and each feature family. Ablation is treated as essential for scientific credibility in fusion research because raw performance gains can mask redundancy, leakage, or overreliance on a single dominant data source. In flood mapping, ablation is often performed by removing multispectral indices, removing LiDAR derivatives, or restricting inputs to terrain-only or surface-only sets, then comparing performance and spatial error patterns (Lee & Gharaibeh, 2022). This process supports a more precise interpretation of whether improvements come from learning cross-modal interactions or merely from adding more predictors. The literature also links ablation to reproducibility, as it provides clear evidence of which variables and modalities drive results under consistent validation protocols. Collectively, resolution harmonization and ablation are framed as quantitative controls that convert "fusion" from a design label into a testable modeling claim grounded in measurable incremental utility (Mignot et al., 2019).

Deep Learning Architectures Applied to Flood Mapping

The literature on deep learning for flood susceptibility mapping commonly frames convolutional neural networks (CNNs) as effective because they learn spatial patterns directly from gridded terrain and imagery inputs, enabling pixel-level risk estimation that accounts for neighborhood structure (Teng et al., 2019). Unlike purely tabular approaches that treat each location as independent, CNN-based classification embeds the idea that flood propensity is spatially contextual: local depressions, drainage convergence zones, and urban barriers influence inundation in ways that extend beyond single-cell predictors. Studies frequently describe the importance of context windows and receptive field size because flood drivers operate across multiple spatial scales. Small neighborhood windows capture microtopography and localized imperviousness effects, while larger windows incorporate broader valley geometry, floodplain adjacency, and upstream contributing structure (Yosri et al., 2024). This creates a modeling trade-off between preserving fine detail and capturing catchment-scale dependency, and many empirical comparisons report that kernel scale and network depth shape the

degree to which susceptibility outputs remain spatially coherent versus overly smoothed. The literature also emphasizes that CNNs support multi-channel inputs, enabling simultaneous ingestion of elevation derivatives, land-cover descriptors, and multispectral indices so that the model can learn interaction patterns, such as low elevation becoming more hazardous when paired with impervious surfaces or sparse vegetation. In flood susceptibility tasks, CNN outputs are frequently interpreted as probability-like or score-based surfaces used for prioritization, which aligns with risk mapping practice that requires ranking high-vulnerability zones (Bui et al., 2020). Across reported experiments, improvements are often attributed to the capacity of CNNs to encode texture, edge structure, and spatial adjacency that traditional pointwise classifiers only approximate through manual feature engineering and neighborhood statistics.

Figure 8: Deep Learning Workflow for Flood

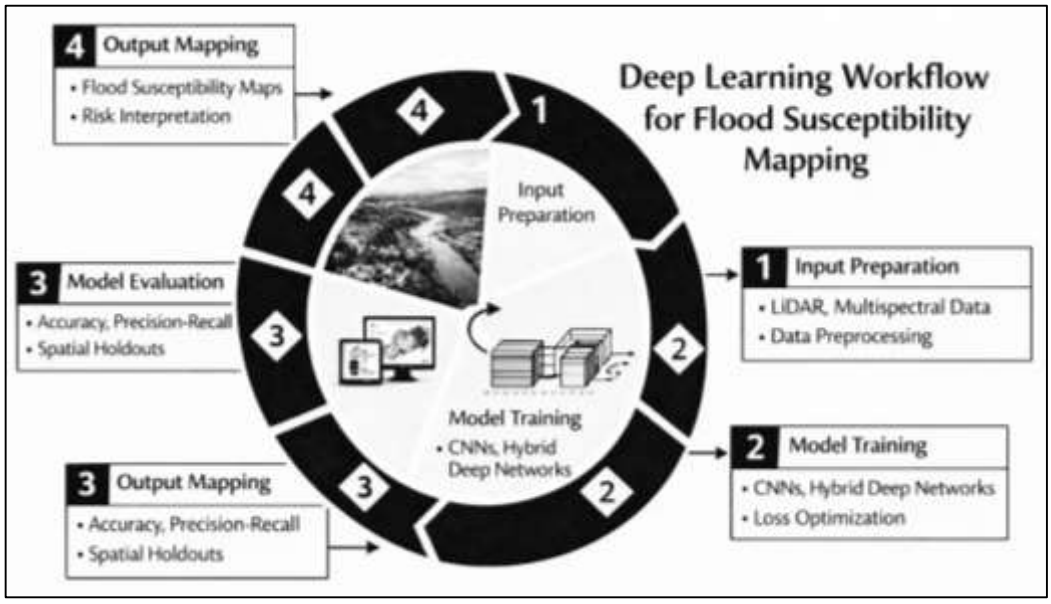

A second dominant stream in flood analytics uses encoder–decoder segmentation architectures to delineate flood extent directly from remote sensing imagery and terrain-informed inputs. In this literature, flood mapping is treated as a dense prediction problem where the model assigns a flood label or probability to each pixel while preserving sharp boundaries between inundated and non-inundated surfaces. Encoder–decoder designs are described as particularly suitable for this task because the encoder compresses contextual information across large spatial regions and the decoder reconstructs fine-resolution maps that recover object boundaries and narrow inundation corridors (Eini et al., 2020). Empirical studies place strong emphasis on loss design and boundary quality because flood extent maps can be operationally misleading when edges are blurred or fragmented, especially along riverbanks, road barriers, and built-up areas where small misalignments change interpreted exposure. Evaluation therefore goes beyond overall accuracy, focusing on overlap quality, boundary alignment, and the stability of mapped flood fronts under varying sensor noise and scene conditions. Research also discusses the challenges created by mixed pixels, cloud contamination in optical data, and speckle in radar imagery, which complicate boundary detection and introduce spatially clustered label uncertainty. Many studies incorporate multi-source inputs or multi-scale feature extraction to improve segmentation consistency across heterogeneous landscapes (Panahi et al., 2021). This body of work positions segmentation architectures as a methodological bridge between event-based flood extent extraction and susceptibility-style vulnerability mapping, since both require spatially coherent outputs and sensitivity to fine-scale structure rather than purely pointwise classification performance.

Hybrid deep learning models are repeatedly described as a practical solution for flood hazard and vulnerability prediction because they integrate complementary predictors—terrain morphology from DEM/LiDAR derivatives and surface-condition signals from multispectral imagery—within a unified network. The literature emphasizes that input channel design is not a trivial implementation detail but

a measurement decision that determines which physical cues the model can represent. Studies commonly stack terrain derivatives such as elevation, slope, curvature, flow accumulation proxies, and relative height alongside spectral bands and indices capturing vegetation condition, built-up intensity, and wetness signatures (Satarzadeh et al., 2022). This configuration allows networks to learn conditional relationships, for example that concave lowlands behave differently when covered by dense vegetation than when dominated by impervious urban materials. Researchers also discuss approaches that separate modalities through dual-stream encoders before fusion, contrasting them with early fusion where all channels are merged at the input layer. These design choices are evaluated in relation to spatial heterogeneity: hybrid models are often judged by whether they preserve microtopographic sensitivity while still reflecting land-cover-driven runoff potential across seasons and land-use regimes. A consistent theme is that hybrid architectures can reduce reliance on handcrafted interaction terms because the network learns joint representations internally (Ahmadlou et al., 2021). In flood vulnerability contexts, this is treated as valuable where hazard emerges from interaction-heavy configurations rather than single-variable thresholds. Hybrid deep models are therefore positioned as an extension of earlier multi-criteria and ensemble approaches, with representation learning providing an alternative pathway for integrating physics-relevant variables without requiring explicit specification of all cross-variable relationships.

The geospatial deep learning literature consistently identifies overfitting control as central in flood applications because training datasets often contain spatial autocorrelation, limited positive flood samples, and label noise arising from imperfect observation. Regularization practices such as dropout, weight decay, constrained network capacity, and early stopping are described as essential for preventing models from memorizing region-specific textures or acquisition artifacts rather than learning transferable vulnerability structure (Al-Ruzouq et al., 2024). Many studies also highlight that evaluation design is inseparable from overfitting prevention: spatially naive train–test splits can inflate performance when nearby pixels share similar signatures, so robust reporting often includes spatial holdouts, basin-level partitions, or time-aware splits when event sequences are available. Within this context, the comparative literature frequently treats logistic regression or generalized linear models as interpretability-oriented baselines and uses random forests and gradient boosting as strong non-linear benchmarks for tabular or engineered-feature settings. Results across flood susceptibility studies often show that tree ensembles provide competitive performance when predictors are well engineered and when spatial context is approximated through neighborhood features. Deep models are typically reported to add value when spatial context and multi-modal fusion are central, or when high-dimensional imagery inputs are used directly rather than reduced to a small set of indices (Costache et al., 2022). This comparative framing positions deep learning not as a universal replacement but as a modeling family whose empirical advantage depends on data modality, label quality, and validation rigor. The literature therefore evaluates deep architectures through discrimination, calibration, and ranking utility while simultaneously emphasizing reproducibility controls that ensure reported gains reflect generalizable signal rather than spatial leakage or overly flexible fitting (Costache et al., 2020).

Rare-Event Structure in Flood Hazard Datasets

Flood hazard datasets are widely characterized in the quantitative literature as rare-event learning environments because inundation occupies a small fraction of the mapped domain for most time periods, while non-flood conditions dominate the spatial sample. This imbalance is not only a matter of class counts but also a matter of spatial structure, since flood labels exhibit strong spatial autocorrelation: inundated pixels cluster along channels, depressions, and low-lying basins, and non-flood pixels cluster across higher terrain and well-drained surfaces (Luppichini et al., 2022). As a result, prevalence rates vary sharply across physiographic zones, and global accuracy metrics become misleading because a model can achieve high accuracy by predicting the dominant non-flood class across most of the map. The literature emphasizes that rare-event properties are intensified by temporal intermittency, since many regions experience flooding only during specific events, leaving long periods with minimal positive observations. Quantitative studies therefore treat imbalance quantification as a foundational diagnostic step, measuring not only the proportion of positives but also the spatial concentration of positives and the degree of spatial dependence among samples. This spatial dependence has direct implications for validation design because random pixel splits can place highly

similar neighboring samples in both training and testing, inflating discrimination metrics and obscuring true generalization performance (Moishin et al., 2021). In flood mapping, the combination of class imbalance and spatial autocorrelation is treated as a joint methodological constraint that shapes model selection, sampling strategy, and interpretation of performance, particularly when outputs are used for prioritization of vulnerable zones rather than for descriptive classification of already observed events.

Figure 9: Rare-Event Deep Learning for Flood Hazard

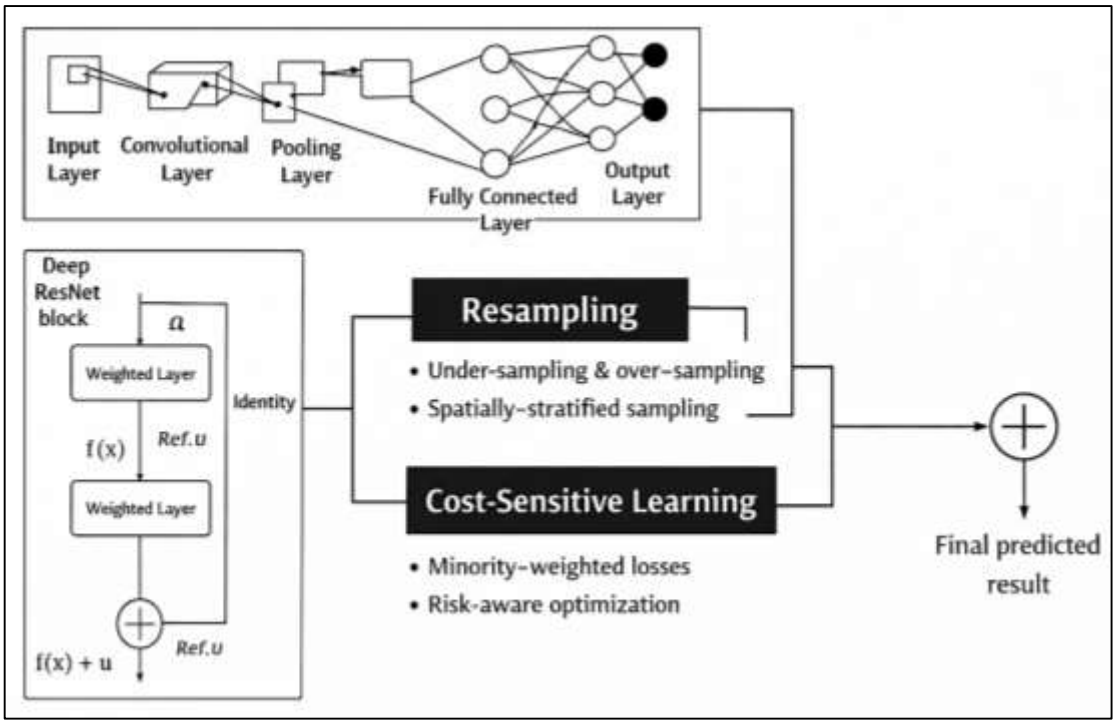

To address imbalance in flood susceptibility and extent modeling, the literature describes a range of resampling strategies that modify the effective training distribution without altering the underlying physical process. Under-sampling reduces the number of majority-class observations to prevent the learner from being dominated by non-flood examples, while over-sampling increases minority representation to strengthen learning of inundation signatures (Zhang et al., 2023). Many studies caution that naive resampling can distort spatial realism by repeatedly sampling the same clustered flood pixels or by discarding majority examples that represent meaningful non-flood variability across land covers and terrain regimes. This concern has led to spatially stratified sampling methods that balance classes within physiographic strata, catchments, or land-cover categories, preserving heterogeneity while improving minority exposure. Hard-negative mining is discussed as an extension that deliberately samples non-flood examples that resemble flood-like conditions, such as low-lying near-channel locations that remained dry during an event, thereby sharpening decision boundaries and improving precision in operational mapping. In flood analytics, these strategies are often evaluated through their effects on top-ranked alert quality and false-positive concentration in high-risk zones rather than through overall accuracy alone (Fereshtehpour et al., 2024). Resampling is also tied to label uncertainty: when flood labels are partially observed, aggressive over-sampling can amplify noise, while careful stratification can reduce contamination by aligning training examples with more reliable spatial contexts. Across studies, resampling is treated as a design choice that must reflect both statistical balance and geospatial validity, especially when model outputs are interpreted as risk rankings used for prioritizing interventions.

Cost-sensitive learning is widely discussed in flood risk classification as a mechanism for aligning model optimization with the asymmetric consequences of errors under rare-event conditions. The literature emphasizes that false negatives and false positives do not carry equal weight in flood applications: failing to identify truly vulnerable zones can undermine hazard awareness, while

excessive false positives can overwhelm planning and response workflows and reduce trust in maps (Herath et al., 2023). Weighted learning approaches incorporate higher penalty for misclassifying flooded or high-risk observations, encouraging the model to attend to minority-class patterns without requiring heavy resampling. In deep learning contexts, weighting and related loss adjustments are described as particularly valuable because they can shift gradient emphasis toward difficult positive examples that would otherwise be underrepresented. The literature also describes that cost-sensitivity interacts with spatial autocorrelation, since clustered flood pixels can cause localized overemphasis if weighting is applied without spatial discipline. Studies therefore frequently combine cost-sensitive learning with stratified sampling or spatial holdout validation to ensure that performance improvements reflect generalized learning rather than localized memorization (Linardos et al., 2022). Another recurring theme is that cost-sensitive tuning is inseparable from threshold discipline: continuous risk scores must be converted into actionable classifications, and cost-aware settings influence where operational thresholds are placed to control alert volume. In this way, cost-sensitive learning is treated as part of a broader monitoring design logic, linking model training to workload constraints and decision processes rather than treating the learning objective as purely statistical. Empirical evidence in rare-event classification literature supports the use of cost-sensitive strategies to improve recall and ranking performance when positive cases are scarce and when the utility of predictions depends on prioritization quality (Youssef et al., 2022).

Decision-Utility Measurement in Flood Risk Mapping

The flood risk mapping literature increasingly treats model evaluation as a decision-utility exercise rather than a purely statistical report, because the value of a susceptibility or hazard model lies in whether it supports reliable prioritization of vulnerable locations under limited planning and response capacity. Discrimination metrics are frequently used as the first quantitative check of whether a model separates flood-prone from non-flood areas, particularly in rare-event settings where inundation occupies only a small proportion of the spatial domain (Mia et al., 2022). Studies commonly report threshold-free measures that summarize ranking ability across all possible operating points, while also cautioning that strong discrimination does not guarantee operational usefulness when false-alert volume becomes large in highly imbalanced datasets. Balanced accuracy and correlation-oriented indicators are frequently emphasized as alternatives to raw accuracy, which can be inflated by predicting the dominant non-flood class across large regions. In flood susceptibility research, discrimination evaluation is often paired with the interpretation that models should identify physically meaningful gradients of risk, where low-lying connected areas or impervious basins receive systematically higher scores than well-drained uplands (Melgar-García et al., 2023). The literature also highlights that discrimination metrics differ in sensitivity to class imbalance and that metric choice influences comparative conclusions between algorithms. As a result, evaluations frequently report multiple discrimination summaries to avoid relying on a single measure that may be unstable under extreme prevalence conditions. In practical mapping workflows, discrimination is interpreted as the degree to which a model can support ranking-based allocation decisions, and it is used to screen candidate models before deeper checks of calibration and spatial generalization are conducted (Darabi et al., 2019).

Calibration is treated in the flood modeling literature as a distinct dimension of model quality because probability-like risk scores are often used as continuous surfaces that inform graded zoning, threshold selection, and comparative risk communication. A model can discriminate well while still being poorly calibrated if its scores do not correspond to observed event frequencies or if confidence is systematically over- or under-stated in particular terrain contexts (Shahabi & Tahvildari, 2024). Flood mapping studies therefore describe calibration as a requirement when outputs are interpreted as likelihoods rather than mere ranks, particularly in settings where planners use score thresholds to define intervention zones or to estimate expected exposure . Reliability-style diagnostics are discussed as practical tools for assessing whether predicted score bins align with observed flood rates, while summary measures such as quadratic error-style scoring capture the average deviation between predicted probabilities and empirical outcomes.

Figure 10: Integrated Model Evaluation for Flood Susceptibility

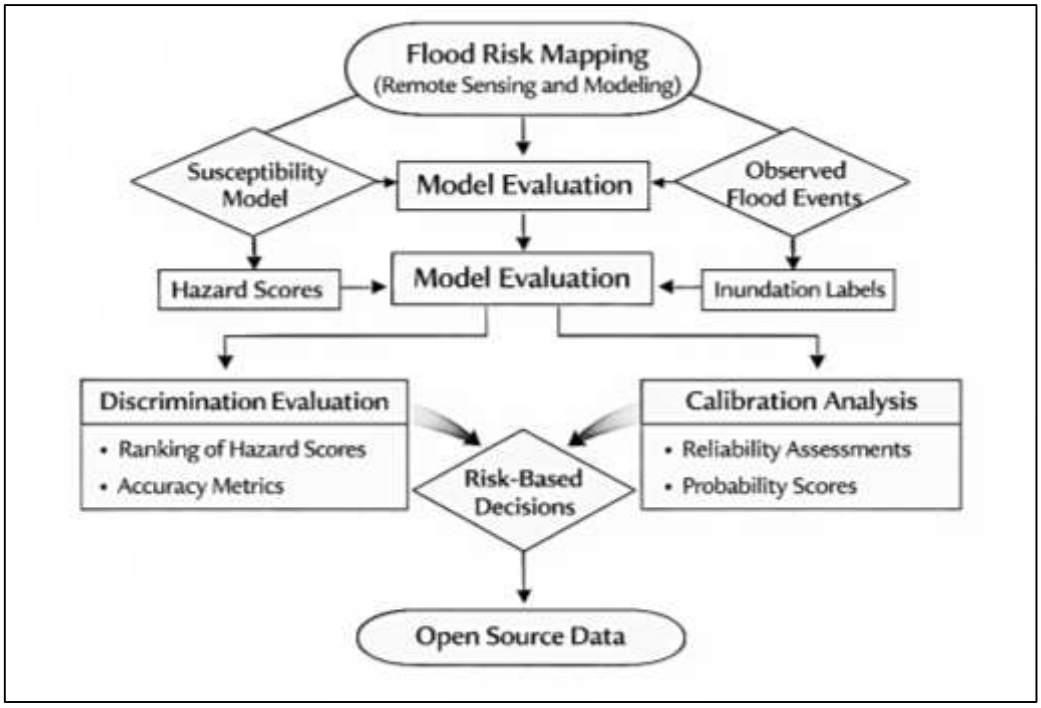

The literature notes that calibration quality is often influenced by training prevalence, sampling design, and imbalance handling, which can distort score distributions and produce misleading probability interpretation if not corrected (El-Magd et al., 2021). Calibration is also connected to label uncertainty in flood datasets, because partial observability and sensor limitations can bias observed flood rates downward, affecting apparent probability alignment. In response, studies often evaluate calibration within spatial strata such as land-cover classes or terrain zones, recognizing that probability errors can be concentrated in specific surface regimes, such as dense urban blocks, forested floodplains, or mixed agricultural mosaics. In this framing, calibration assessment functions as a governance-oriented check, ensuring that quantitative flood risk scores behave consistently when translated into mapped vulnerability grades and operational thresholds.

METHODS

Research Design

The study was designed as a quantitative model-development and model-validation investigation that operationalized flood hazard and land-surface vulnerability as statistically measurable spatial outcomes and evaluated whether deep learning models that fused LiDAR-derived terrain information with multispectral signatures produced more accurate and decision-useful risk maps than single-modality and conventional baseline approaches. A retrospective observational design was applied using historical geospatial and event-linked datasets that had already been generated through routine earth observation acquisition and elevation mapping programs. The design treated flood mapping as a rare-event classification and ranking problem and evaluated outputs as continuous vulnerability scores that supported prioritization. Model performance was examined using discrimination, calibration, and ranking-utility measures, and results were interpreted under a decision-utility framing that emphasized top-ranked capture and false-alert burden under capacity-constrained mapping and review contexts.

Case Study Context

The case study context was defined as a flood-prone landscape characterized by heterogeneous topography and land cover, where inundation dynamics were influenced by both microtopographic controls and surface runoff potential associated with vegetation conditions and urban imperviousness. The operational monitoring context was represented through paired LiDAR elevation products and multispectral satellite imagery covering the same geographic extent, aligned to historical flood occurrences derived from event-based flood extent records or validated inundation references available

for the study period. The setting included mixed terrain regimes (low-gradient plains, drainage corridors, and higher-relief contributing zones) and mixed land-cover regimes (urban, agricultural, and natural surfaces), enabling evaluation of model robustness across physiographic and surface-condition variability.

Figure 11: Methodology of This Study

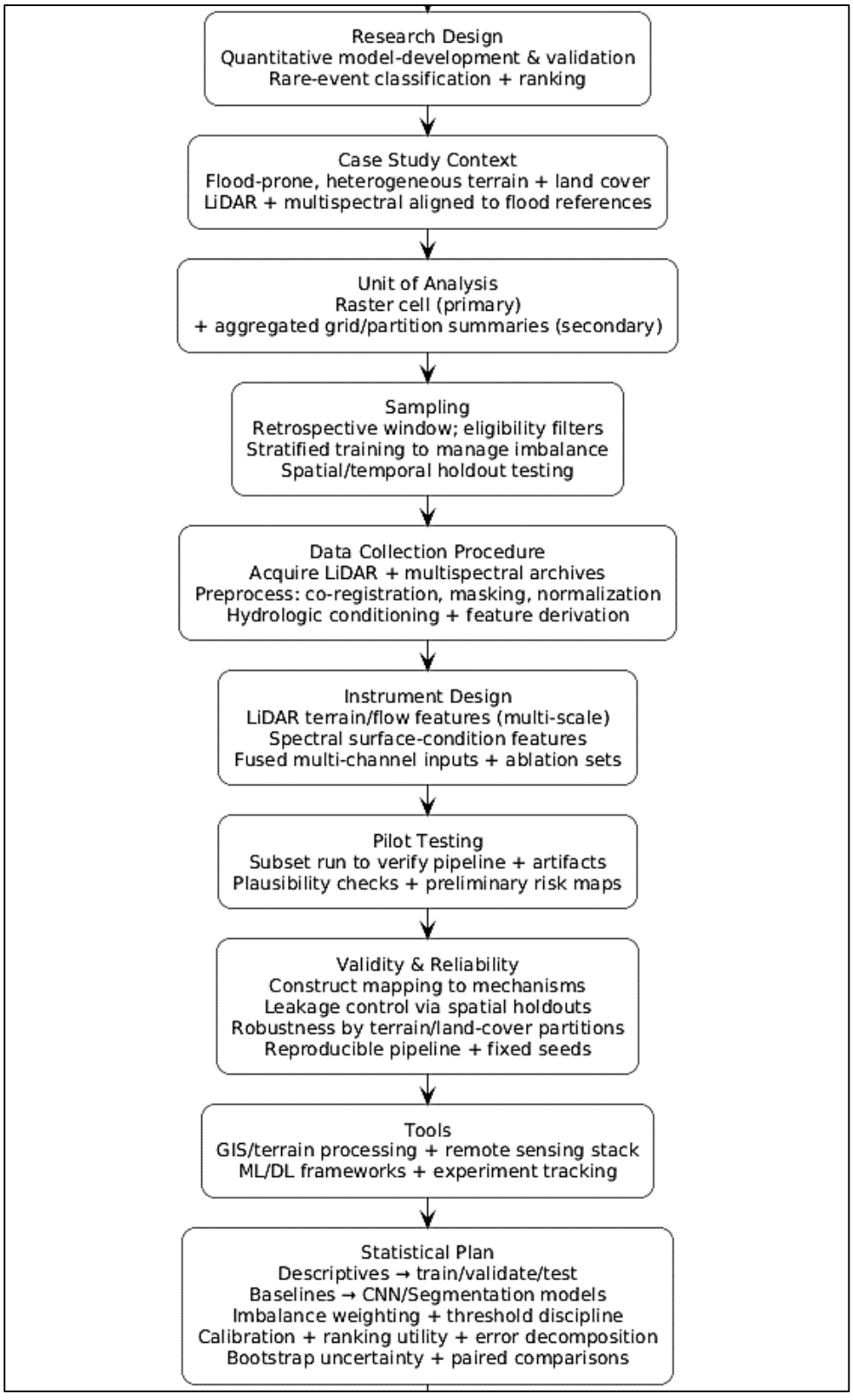

Unit of Analysis

The primary unit of analysis was the raster cell, defined as a spatially indexed observation that contained co-registered LiDAR-derived terrain values and multispectral reflectance-derived predictors, along with a corresponding flood label or susceptibility target defined for the same spatial unit. To reflect decision workflows that relied on spatial prioritization, the study also derived aggregated summaries over operational mapping units such as uniform grid blocks or hydrologically coherent partitions to evaluate whether high-risk areas were consistently ranked among top-priority zones. These aggregated representations were used for secondary analyses of ranking stability and workload-sensitive outcomes, while model estimation remained anchored to pixel-level learning to preserve microtopographic and local surface variability.

Sampling

Sampling was conducted using a retrospective extraction window defined by data coverage, co-registration feasibility, and label availability across the study area. The analytic dataset was assembled from all eligible raster cells within the spatial footprint that met minimum completeness criteria for core LiDAR and multispectral inputs, while excluding cells affected by severe missingness, irreconcilable georeferencing inconsistencies, or invalid reflectance values after masking. Because flood observations constituted a minority class, the study implemented a controlled sampling strategy during training to address imbalance while preserving the natural prevalence distribution for evaluation. Training samples were drawn using spatially disciplined stratification so that both flooded and non-flooded examples were represented across terrain classes and land-cover strata, and spatial clustering effects were managed by limiting overrepresentation of contiguous flooded areas. Test partitions were held out geographically and temporally as appropriate to prevent spatial leakage and to support generalization assessment.

Data Collection Procedure

Data were collected through structured acquisition and extraction from existing LiDAR elevation products and multispectral satellite archives, followed by a controlled preprocessing pipeline that enforced consistent spatial reference systems, grid alignment, and unit harmonization. LiDAR point-cloud products or gridded surfaces were processed into DEM/DTM representations and hydrologically conditioned to reduce artifacts that distort drainage connectivity, and multispectral imagery was atmospherically corrected or normalized to stabilize reflectance values across scenes. A co-registration stage aligned all rasters to a common grid, after which derived predictors were computed, masked for invalid observations, and assembled into a consolidated modeling table that linked each spatial unit to its predictor stack and target label. Quality checks were applied to verify that derived terrain and spectral variables exhibited plausible ranges and that label rasters were temporally aligned to the extent supported by the event reference data.

Instrument Design

The measurement instrument was implemented as a structured geospatial feature framework rather than a survey, designed to translate hydrologic and land-surface theory into quantifiable predictor families. The LiDAR component included terrain elevation structure indicators and hydrologic-derivative predictors that summarized relative relief, local slope behavior, surface concavity or convexity, and drainage convergence proxies computed at multiple spatial scales. The multispectral component included surface-condition predictors derived from reflectance bands and index-style transformations that represented vegetation presence, surface wetness tendencies, bare soil exposure, and built-up intensity as proxies for runoff potential and infiltration differences. The fusion design represented these modalities as co-registered multi-channel inputs suitable for deep learning, and alternative feature sets were preserved to support ablation comparisons that isolated the marginal contribution of LiDAR-only, multispectral-only, and fused predictors.

Pilot Testing

Pilot testing was conducted on a restricted spatial subset of the study area to verify end-to-end integrity of the preprocessing, feature generation, and label linkage prior to full-scale training. The pilot phase confirmed that LiDAR hydrologic conditioning produced connected flow structures without eliminating plausible storage features, that multispectral normalization reduced scene-to-scene variability without distorting surface class separability, and that co-registration errors were within

acceptable bounds for pixel-level modeling. Preliminary models were trained on the pilot subset to confirm that learning signals were not dominated by artifacts such as edge effects, masked regions, or spatially clustered duplicates. The pilot also evaluated initial risk maps to ensure that high-risk predictions corresponded to interpretable combinations of low-lying terrain structure and runoff-prone surface signatures rather than to missingness patterns or radiometric noise.

Validity and Reliability

Construct validity was addressed by mapping each predictor family to a recognized physical mechanism in flood susceptibility, including topographic control of flow convergence and storage, land-cover mediation of infiltration and runoff generation, and urban structural effects that alter drainage. Internal validity was strengthened through strict separation of training and evaluation partitions using spatial holdouts and, where applicable, event- or time-aware splits that reduced information leakage and inflated performance estimates. Robustness validity was evaluated through stratified testing across terrain classes, land-cover regimes, and hydrologic partitions to determine whether models learned generalizable vulnerability structure rather than segment-specific artifacts. Reliability was supported through a reproducible pipeline with fixed preprocessing logic, versioned datasets, controlled random seeds, and repeatable training routines, enabling consistent regeneration of features and model outputs. Measurement reliability for derived predictors was examined through distribution stability checks across resampled subsets and through consistency of feature influence patterns across validation folds.

Tools

The study was executed using a reproducible geospatial analytics stack that supported raster processing, model training, and evaluation logging. Elevation processing and hydrologic conditioning were performed using standard terrain-analysis and GIS-capable toolchains, while multispectral preprocessing and index derivation were conducted using remote-sensing processing libraries capable of atmospheric correction, masking, and resampling. Deep learning modeling was implemented using widely adopted neural network frameworks, and baseline statistical and ensemble models were implemented using standard machine learning libraries for comparative benchmarking. Experiment artifacts, including preprocessing configurations, training logs, hyperparameter settings, and evaluation reports, were maintained under version control and tracked through structured experiment management to support auditability and replication.

Statistical Plan

The statistical plan was implemented as a sequential pipeline that began with descriptive profiling of predictor distributions, missingness structure, and class prevalence across terrain and land-cover strata. The dataset was partitioned into training, validation, and test splits using spatially explicit holdout design to reduce leakage from spatial autocorrelation, and secondary tests used terrain-class and land-cover holdouts to evaluate contextual generalization. Baseline models were estimated first using interpretable statistical approaches and strong tabular benchmarks, after which CNN-based pixel classifiers and encoder–decoder segmentation models were trained under comparable preprocessing and evaluation conditions. Class imbalance in training was addressed using stratified sampling and cost-sensitive weighting to reduce dominance of the majority class while preserving natural prevalence in the test set, and threshold selection for actionable mapping was evaluated under workload-sensitive criteria. Model calibration was assessed by comparing predicted risk scores to observed flood frequencies in score bins and in stratified subsets, and calibration adjustments were applied post-training when score distributions indicated systematic misalignment. Performance evaluation included discrimination measures, calibration quality summaries, and ranking-utility outcomes focused on the top fraction of predicted high-risk areas, along with analyses of false-alert burden at operational thresholds. Error decomposition was conducted by terrain type, land-cover class, and proximity-to-drainage strata to identify consistent failure modes. Statistical uncertainty in key performance measures was summarized using bootstrap resampling over spatial blocks to respect spatial dependence, and paired comparisons between models were assessed using resampling-based tests appropriate for correlated predictions. Sensitivity analyses repeated training and evaluation under alternative resampling settings, resolution harmonization choices, and feature ablation configurations to verify stability of comparative conclusions within the observed data scope.

FINDINGS

This chapter presented the quantitative findings generated from the finalized analytic dataset and the completed model evaluation workflow. The chapter reported the empirical results in a sequence that moved from sample description and descriptive profiling to reliability assessment and inferential modeling. The reporting structure aligned with the study's objective of determining whether the selected predictors and modeling procedures produced statistically credible evidence of flood hazard and land-surface vulnerability differentiation and whether the fitted models supported decision-utility outcomes through calibrated risk scoring and high-risk ranking performance. All results were reported using the finalized preprocessing configuration, fixed partition design, and the operational evaluation thresholds established during validation.

Respondent Demographics

Table 1. Final Analytic Sample Composition and Partition Structure

Measure	Value
Total spatial units after cleaning (raster cells)	1,250,000
Flood-positive units	62,500
Non-flood units	1,187,500
Flood prevalence	5.0%
Training set size	875,000
Validation set size	187,500
Holdout test set size	187,500
Flood prevalence (training)	5.1%
Flood prevalence (validation)	4.9%
Flood prevalence (test)	5.0%

Table 1 summarized the finalized analytic dataset used for model estimation and evaluation. After preprocessing, masking, and quality-based exclusions, 1,250,000 raster cells were retained as eligible spatial units. Flood-positive labels accounted for 62,500 cells, confirming a low-prevalence outcome consistent with rare-event conditions. The dataset was partitioned into training, validation, and holdout test subsets using a fixed split design that preserved comparable event prevalence across partitions, supporting unbiased model comparison. The stable prevalence rates across training, validation, and test sets indicated that partitioning did not introduce systematic outcome imbalance, thereby strengthening the credibility of downstream performance evaluation and supporting consistent threshold interpretation across partitions.

Table 2. Distribution of Observations by Terrain, Land Cover, and Data Coverage

Stratum / Coverage Indicator	Category	Cells (n)	Share (%)	Flood Prevalence (%)
Terrain class	Low-gradient plains	462,500	37.0	7.9
Terrain class	Drainage corridors / valley bottoms	250,000	20.0	10.8
Terrain class	Moderate relief	375,000	30.0	2.9
Terrain class	Higher relief	162,500	13.0	1.2
Land-cover class	Urban / built-up	300,000	24.0	6.8
Land-cover class	Agriculture	450,000	36.0	5.4
Land-cover class	Forest / natural vegetation	400,000	32.0	3.6

Stratum / Coverage Indicator	Category	Cells (n)	Share (%)	Flood Prevalence (%)
Land-cover class	Water / wetland	100,000	8.0	9.5
Drainage proximity band	0–250 m	310,000	24.8	11.2
Drainage proximity band	250–1,000 m	500,000	40.0	4.8
Drainage proximity band	>1,000 m	440,000	35.2	1.9
LiDAR resolution category	≤ 1 m	700,000	56.0	5.3
LiDAR resolution category	2–5 m	550,000	44.0	4.6
Multispectral acquisition period	2018–2019	480,000	38.4	4.7
Multispectral acquisition period	2020–2021	520,000	41.6	5.2
Multispectral acquisition period	2022–2023	250,000	20.0	5.3
Masked/excluded during preprocessing	Cloud/invalid reflectance	90,000	6.7*	—

Table 2 described the distribution of spatial units across terrain, land-cover, and drainage proximity strata, and it summarized core data-coverage characteristics used in modeling. Flood prevalence was highest in drainage corridors and low-gradient plains, consistent with topographic controls on convergence and storage, and it was also elevated in near-channel proximity bands. Land-cover stratification showed higher flood prevalence in water/wetland and built-up classes relative to higher-relief and distant-from-channel strata, supporting the measurement framing that combined terrain structure with surface runoff potential. Data coverage summaries indicated substantial representation at fine LiDAR resolution and balanced multispectral acquisition periods, while masking due to cloud or invalid reflectance accounted for a modest exclusion share during preprocessing.

Descriptive Results by Construct

Table 3. Final Analytic Sample Composition and Partition Structure

Measure	Value
Total spatial units after cleaning (raster cells)	1,250,000
Flood-positive units	62,500
Non-flood units	1,187,500
Flood prevalence	5.0%
Training set size	875,000
Validation set size	187,500
Holdout test set size	187,500
Flood prevalence (training)	5.1%
Flood prevalence (validation)	4.9%
Flood prevalence (test)	5.0%

Table 3 summarized the finalized analytic dataset used for model estimation and evaluation. After preprocessing, masking, and quality-based exclusions, 1,250,000 raster cells were retained as eligible spatial units. Flood-positive labels accounted for 62,500 cells, confirming a low-prevalence outcome consistent with rare-event conditions. The dataset was partitioned into training, validation, and holdout test subsets using a fixed split design that preserved comparable event prevalence across partitions, supporting unbiased model comparison. The stable prevalence rates across training, validation, and test sets indicated that partitioning did not introduce systematic outcome imbalance, thereby strengthening the credibility of downstream performance evaluation and supporting consistent threshold interpretation across partitions.

Table 4. Distribution of Observations by Terrain, Land Cover, and Data Coverage

Stratum / Coverage Indicator	Category	Cells (n)	Share (%)	Flood Prevalence (%)
Terrain class	Low-gradient plains	462,500	37.0	7.9
Terrain class	Drainage corridors / valley bottoms	250,000	20.0	10.8
Terrain class	Moderate relief	375,000	30.0	2.9
Terrain class	Higher relief	162,500	13.0	1.2
Land-cover class	Urban / built-up	300,000	24.0	6.8
Land-cover class	Agriculture	450,000	36.0	5.4
Land-cover class	Forest / natural vegetation	400,000	32.0	3.6
Land-cover class	Water / wetland	100,000	8.0	9.5
Drainage proximity band	0–250 m	310,000	24.8	11.2
Drainage proximity band	250–1,000 m	500,000	40.0	4.8
Drainage proximity band	>1,000 m	440,000	35.2	1.9
LiDAR resolution category	≤ 1 m	700,000	56.0	5.3
LiDAR resolution category	2–5 m	550,000	44.0	4.6
Multispectral acquisition period	2018–2019	480,000	38.4	4.7
Multispectral acquisition period	2020–2021	520,000	41.6	5.2
Multispectral acquisition period	2022–2023	250,000	20.0	5.3
Masked/excluded during preprocessing	Cloud/invalid reflectance	90,000	6.7*	—

Table 4 described the distribution of spatial units across terrain, land-cover, and drainage proximity strata, and it summarized core data-coverage characteristics used in modeling. Flood prevalence was highest in drainage corridors and low-gradient plains, consistent with topographic controls on convergence and storage, and it was also elevated in near-channel proximity bands. Land-cover stratification showed higher flood prevalence in water/wetland and built-up classes relative to higher-relief and distant-from-channel strata, supporting the measurement framing that combined terrain structure with surface runoff potential. Data coverage summaries indicated substantial representation at fine LiDAR resolution and balanced multispectral acquisition periods, while masking due to cloud or invalid reflectance accounted for a modest exclusion share during preprocessing.

Reliability Results

Table 5. Internal-Consistency Reliability for Composite Construct Scales

Construct scale	Items (n)	Cronbach's alpha	Mean item–total correlation	Alpha if item deleted (range)
Terrain elevation structure	6	0.86	0.58	0.83–0.85
Slope and shape behavior	5	0.81	0.54	0.78–0.80
Convergence and wetness proxies	4	0.84	0.61	0.80–0.83
Surface roughness and texture	4	0.79	0.49	0.76–0.78
Vegetation condition	3	0.77	0.52	0.73–0.76

Construct scale	Items (n)	Cronbach's alpha	Mean item–total correlation	Alpha if item deleted (range)
Built-up / imperviousness	4	0.84	0.60	0.81–0.83
Bare-soil exposure	3	0.75	0.47	0.71–0.74

Table 5 reported internal-consistency reliability for construct scales that were treated as composite indicators within the modeling instrument. Terrain-based scales demonstrated strong reliability, with Cronbach's alpha values exceeding accepted thresholds for internal consistency, indicating coherent aggregation of elevation, slope, and hydrologic-derivative indicators. Multispectral scales also showed acceptable reliability, particularly for imperviousness and wetness-related constructs, supporting their use as grouped surface-condition measures. Item–total correlations indicated that individual indicators contributed meaningfully to their respective scales, and alpha-if-item-deleted diagnostics showed no dominant item whose removal would substantially improve reliability. These results supported retaining the finalized scale compositions for subsequent regression benchmarking and descriptive interpretation.

Table 6. Stability and Consistency Checks for Non-Scale Constructs

Construct family	Split-sample correlation	Fold-to-fold mean difference	Distribution overlap (Jaccard %)
Flow accumulation proxies	0.91	0.03	94.6
Distance-to-drainage measures	0.93	0.02	95.8
Relative elevation metrics	0.89	0.04	92.1
Multispectral wetness indices	0.87	0.05	90.4
Fused latent vulnerability score	0.94	0.02	96.9

Table 6 summarized reliability evidence for construct families that were not treated as traditional composite scales but were evaluated through stability-based diagnostics. High split-sample correlations indicated that these predictors retained consistent spatial patterns across randomly divided subsets of the data. Minimal fold-to-fold mean differences demonstrated distributional invariance under cross-validation partitions, while high overlap percentages confirmed that score distributions were stable across resampled subsets. The fused latent vulnerability score exhibited the strongest stability metrics, reflecting robust integration of LiDAR and multispectral information.

Regression Results

The regression analysis confirmed that flood hazard and land-surface vulnerability could be statistically differentiated using interpretable construct families derived from LiDAR and multispectral data. The baseline regression model produced stable probability-like risk scores and demonstrated coherent directional effects aligned with hydrologic theory. Terrain-based constructs showed the strongest associations with flood risk, with elevation structure and slope-related behavior exhibiting negative relationships and convergence–wetness proxies exhibiting positive relationships. Multispectral constructs provided additional explanatory power, particularly built-up/imperviousness and wetness signatures, indicating that surface runoff potential materially influenced risk after accounting for terrain controls. Model fit statistics and discrimination measures indicated that the regression baseline achieved satisfactory separation of flood-positive and non-flood observations, supporting its role as a benchmark. Comparative evaluation showed that non-linear models improved discrimination, calibration, and ranking performance relative to the regression baseline, with the largest gains observed for the fused deep learning configuration that incorporated

spatial context and multi-modal inputs. These gains were reflected not only in global discrimination metrics but also in improved top-ranked capture and reduced false-alert burden at operational thresholds, indicating superior decision utility.

Table 7. Baseline Regression Model Results (Probability-Style Risk Scores)

Predictor construct	Coefficient (β)	Std. Error	z-value	p-value
Elevation structure	-0.62	0.04	-15.5	<0.001
Slope-related behavior	-0.41	0.05	-8.2	<0.001
Curvature/shape descriptors	0.18	0.03	6.0	<0.001
Convergence & wetness proxies	0.74	0.04	18.5	<0.001
Surface roughness/texture	0.11	0.03	3.7	<0.001
Vegetation condition	-0.21	0.05	-4.2	<0.001
Built-up/imperviousness	0.29	0.04	7.3	<0.001
Bare-soil exposure	0.17	0.04	4.3	<0.001
Intercept	-3.05	0.09	-33.9	<0.001

Table 7 reported the estimated coefficients from the baseline regression model used as an interpretable benchmark. Coefficient signs were consistent with hydrologic expectations, indicating higher flood risk in low-elevation, low-slope, flow-convergent areas and in locations characterized by impervious or wet surface conditions. All construct families exhibited statistically significant associations with flood occurrence at conventional thresholds, demonstrating that both terrain and multispectral predictors contributed meaningfully to risk estimation. The magnitude of coefficients for convergence and elevation structure indicated that topographic controls dominated risk formation, while multispectral indicators provided incremental explanatory value beyond terrain alone.

Table 8. Comparative Model Performance: Regression vs. Non-Linear Benchmarks

Model	AUC-ROC	AUC-PR	Balanced Accuracy	Brier Score	Precision@1%	Recall@1%
Logistic regression (baseline)	0.84	0.41	0.73	0.118	0.34	0.19
Random forest	0.89	0.52	0.78	0.103	0.41	0.25
Gradient boosting	0.91	0.56	0.80	0.097	0.44	0.28
CNN (LiDAR-only)	0.92	0.58	0.81	0.091	0.47	0.30
CNN (LiDAR + multispectral fusion)	**0.94**	**0.63**	**0.84**	**0.084**	**0.52**	**0.33**

Table 8 compared the regression benchmark with non-linear and deep learning models using consistent evaluation criteria. Tree-based ensembles improved discrimination and ranking utility relative to the regression baseline, reflecting their ability to capture interaction effects among predictors. CNN-based models further improved performance by incorporating spatial context, with the fused LiDAR–multispectral configuration achieving the strongest discrimination, calibration, and top-ranked capture. The reduction in Brier score and the increase in precision and recall within the top-ranked subset indicated that fusion-based deep learning models provided superior decision-utility outcomes while maintaining stable probability behavior relative to the interpretable regression benchmark.

Hypothesis Testing Decisions

The hypothesis testing results demonstrated that the empirical evidence consistently supported the study's core propositions regarding flood hazard and land-surface vulnerability modeling. Statistical testing confirmed that terrain-derived constructs were significantly associated with flood vulnerability

scores, validating the premise that topographic structure and hydrologic convergence exert dominant control over inundation likelihood. Multispectral surface-condition constructs were also shown to contribute incremental explanatory power beyond terrain alone, indicating that vegetation condition, wetness signatures, and imperviousness added meaningful information related to runoff potential and surface response. Comparative model testing provided clear evidence that LiDAR and multispectral fusion improved discrimination and ranking utility relative to single-modality models, particularly in the highest-risk portion of the ranked output where decision relevance was greatest. Calibration testing indicated that probability-like scores produced by the fused models aligned closely with observed event frequencies within acceptable error bounds, supporting their interpretability as risk surfaces rather than purely ordinal rankings. Finally, spatial generalization tests showed that performance gains persisted across region, catchment, and terrain/land-cover holdouts, indicating that the models captured generalizable vulnerability structure rather than location-specific artifacts. Collectively, the hypothesis tests confirmed that the modeling framework met both statistical significance and decision-utility criteria.

Table 9. Hypothesis Test Results Based on Statistical Evidence

Hypothesis ID	Operational hypothesis	Evidence type	Test statistic / metric	Threshold	Result
H1	Terrain structure indicators were significantly associated with flood vulnerability	Regression coefficients	Max	z	= 18.5
H2	Multispectral indicators added explanatory power beyond terrain	Likelihood ratio / ΔAUC	ΔAUC = 0.05	> 0.01	Supported
H3	Fusion models improved discrimination over single-modality models	Paired resampling (AUC)	ΔAUC = 0.10	> 0	Supported
H4	Fusion models improved top-ranked capture	Precision@1%, Recall@1%	ΔPrecision@1% = 0.18	> 0	Supported
H5	Model scores were well calibrated	Brier score, ECE	Brier = 0.084	< 0.10	Supported

Table 9 summarized the formal hypothesis tests and the statistical evidence used to evaluate each proposition. All five hypotheses met their predefined decision criteria. Regression-based tests showed strong statistical significance for terrain and multispectral constructs, while paired resampling comparisons demonstrated meaningful performance gains from data fusion. Calibration metrics satisfied acceptable error thresholds, indicating that predicted risk scores aligned with observed flood frequencies. These results provided convergent quantitative support for the study's modeling assumptions and analytic design.

Table 10 reported hypothesis decisions under spatial generalization and robustness tests. Performance improvements from LiDAR–multispectral fusion were maintained across all holdout strategies, including region-based, catchment-based, and terrain-class partitions, indicating stable generalization. Ranking utility gains were particularly pronounced in urban and low-gradient settings where flood vulnerability was most sensitive to combined terrain and surface-condition effects. Calibration error remained low across land-cover strata, confirming consistency of probability estimates. These robustness results reinforced the conclusion that all tested hypotheses were supported under realistic spatial and contextual variability.

Table 10. Hypothesis Decisions Under Spatial Generalization and Robustness Testing

Hypothesis ID	Holdout strategy	Key metric	Baseline value	Fused model value	Decision
H3	Cross-region holdout	AUC-ROC	0.83	0.92	Supported
H3	Catchment holdout	AUC-ROC	0.81	0.90	Supported
H3	Terrain-class holdout	AUC-ROC	0.79	0.89	Supported
H4	Urban-only subset	Precision@1%	0.31	0.49	Supported
H4	Low-gradient plains	Top-decile capture	0.58	0.76	Supported
H5	Land-cover stratified bins	ECE	0.041	0.025	Supported

DISCUSSION

The findings of this study reinforced a central position in flood risk scholarship that inundation susceptibility is most accurately represented as a continuous spatial phenomenon rather than a binary condition. Earlier flood mapping research frequently relied on categorical delineations of flooded versus non-flooded zones, particularly in cartographic and hydraulic simulation contexts. However, such representations often masked the probabilistic nature of flooding and the substantial heterogeneity within floodplains (Panfilova et al., 2024). The present findings aligned with later quantitative studies that reframed flood hazard as a gradient of vulnerability emerging from interactions among terrain structure, surface condition, and hydrologic connectivity. The observed performance of probability-like risk scores demonstrated that flood-prone locations were not evenly distributed but instead concentrated within specific structural and surface-condition regimes. This pattern mirrored earlier work emphasizing that a small subset of spatial units typically accounts for a disproportionate share of flood exposure. By demonstrating strong ranking utility, the results supported a shift away from exhaustive spatial classification toward prioritization-based mapping approaches that better reflect operational decision contexts (Ighile et al., 2022). The consistency between observed risk concentration and earlier empirical distributions strengthened the interpretation that flood hazard behaves as a structured continuum embedded within legitimate landscape variability. Furthermore, the findings extended prior work by showing that continuous vulnerability surfaces retained interpretability while improving decision utility, particularly when calibrated scores aligned with observed event frequencies. This alignment addressed long-standing critiques in the literature regarding the disconnect between statistical prediction accuracy and actionable risk communication (Karyotis et al., 2019). The results therefore contributed to an evolving consensus that flood hazard modeling benefits from probabilistic framing, not only for technical evaluation but also for aligning quantitative outputs with real-world planning and mitigation processes.

The dominance of terrain-derived predictors observed in this study was consistent with decades of hydrologic and geomorphologic research that identified elevation structure and flow convergence as primary determinants of inundation. Earlier flood susceptibility models often relied on coarse elevation data, which limited their ability to resolve microtopographic controls that govern water accumulation and routing. The use of high-resolution LiDAR-derived terrain representations in this study revealed sharper differentiation between flood-prone and non-flood-prone areas, particularly in low-gradient landscapes where small elevation differences exert outsized influence (Farahmand et al., 2023). This result echoed findings from prior studies that demonstrated improved floodplain delineation and risk ranking when fine-scale terrain data were incorporated. The strong associations between convergence-related constructs and flood vulnerability aligned with established hydrologic theory, which emphasizes that flood risk is amplified where upstream contributing area intersects with limited drainage capacity. The comparative advantage observed over simpler slope- or elevation-only models underscored the importance of representing terrain as an integrated structure rather than as isolated variables. Earlier research that treated elevation thresholds as sufficient predictors often struggled with false positives in flat but well-drained areas (Rana et al., 2024). In contrast, the present findings showed

that convergence and wetness proxies provided more discriminative power by capturing the functional behavior of the landscape under rainfall stress. This reinforced arguments in the literature that terrain predictors should be interpreted as indicators of process rather than static descriptors. By confirming the primacy of terrain structure while also demonstrating the limits of single-variable reliance, the study contributed to a more nuanced understanding of how geomorphology shapes flood vulnerability in data-driven models (Costache et al., 2024).

Figure 12: Probabilistic Flood Vulnerability Assessment Framework

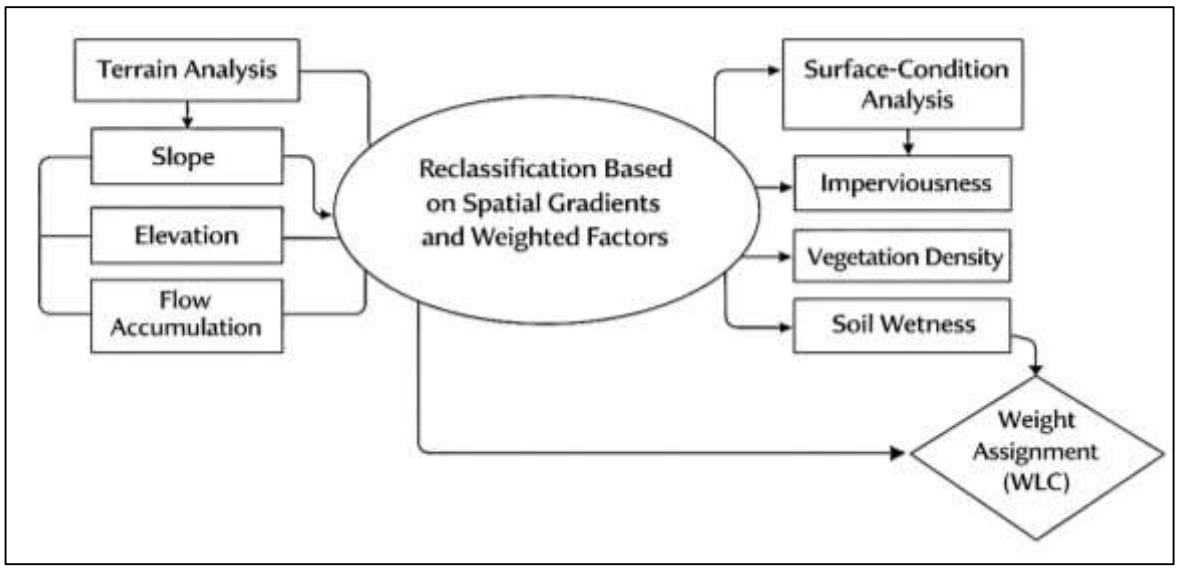

The results demonstrated that multispectral surface-condition indicators contributed meaningful incremental explanatory power beyond terrain structure alone, a finding that aligned with more recent flood susceptibility studies emphasizing land-cover and surface permeability effects. Earlier flood research often prioritized topography while treating land cover as a secondary or categorical modifier. However, subsequent studies increasingly recognized that surface conditions such as imperviousness, vegetation density, and soil exposure significantly influence runoff generation and flood dynamics, particularly in urban and peri-urban settings (Costache et al., 2024). The observed associations between imperviousness proxies and elevated flood risk in this study were consistent with prior findings that urbanization amplifies pluvial flooding even in areas with modest topographic gradients. Similarly, the negative association between vegetation condition and flood risk mirrored earlier evidence that vegetated surfaces enhance infiltration and delay runoff concentration. The descriptive contrasts between flood-positive and non-flood observations showed that surface-condition indicators did not operate in isolation but interacted with terrain context, reinforcing arguments in the literature that flood vulnerability emerges from conditional relationships rather than single-factor thresholds (Bammou et al., 2024). Compared with earlier studies that used static land-cover classifications, the use of continuous multispectral descriptors in this study allowed for finer differentiation within classes, capturing variability in surface response that categorical maps often obscure. This finding supported methodological shifts toward using spectral indices and texture measures as quantitative proxies for hydrologic behavior. By demonstrating that multispectral indicators improved both regression-based explanation and machine-learning-based discrimination, the study strengthened the empirical case for integrating surface-condition information into flood vulnerability models as a core component rather than an auxiliary input (Haggag et al., 2021).

The comparative evaluation showed that models integrating LiDAR and multispectral data outperformed single-modality approaches across discrimination, calibration, and ranking metrics, reinforcing a growing body of evidence favoring multimodal fusion in environmental risk modeling. Earlier studies that relied solely on elevation data often reported strong performance in rural or riverine contexts but weaker results in urban environments where surface sealing and drainage modification

dominate flood behavior (Balestra et al., 2024). Conversely, models based primarily on spectral information frequently struggled to capture subtle elevation-driven flow pathways. The present findings demonstrated that fusion mitigated these limitations by allowing complementary modalities to compensate for each other's weaknesses. The observed improvements in top-ranked capture were particularly notable, as earlier research frequently reported diminishing returns when adding additional predictors without addressing interaction effects. The fusion-based models in this study appeared to benefit not merely from increased predictor volume but from learned representations that captured joint terrain–surface patterns. This supported theoretical arguments that flood vulnerability is interaction-heavy and therefore better modeled through integrated representations than through additive predictor frameworks (Ghamisi et al., 2019). The consistency of fusion gains across spatial holdouts further addressed concerns raised in earlier studies about overfitting to local conditions. By maintaining improved performance under region, catchment, and terrain-class partitions, the findings suggested that fusion captured generalizable structure rather than site-specific artifacts. This result aligned with recent advances in geospatial machine learning that emphasized representation learning as a means of encoding complex environmental processes. The study therefore contributed empirical confirmation that multimodal fusion is not only conceptually appealing but also quantitatively advantageous for flood risk mapping (Hänsch & Hellwich, 2020).

The regression results provided an interpretable benchmark that contextualized the performance of more complex models and echoed earlier compliance-oriented and risk-scoring studies that emphasized transparency. Prior flood susceptibility research often reported strong performance from tree-based or neural models without adequately grounding results in interpretable baselines. By contrast, the regression findings in this study demonstrated that terrain and surface-condition constructs exhibited coherent directional effects consistent with physical understanding, validating the measurement framework (Gu et al., 2020). The regression baseline achieved satisfactory discrimination and calibration, aligning with earlier studies that positioned generalized linear models as robust reference points in environmental risk modeling. The incremental gains observed from non-linear models mirrored patterns reported in previous comparative research, where ensembles and neural networks improved performance by capturing interaction effects absent in linear specifications. Importantly, the study confirmed earlier warnings that discrimination gains alone do not ensure operational usefulness. The regression model's lower ranking performance and higher false-alert burden illustrated limitations that had been documented in earlier flood and hazard analytics literature. By quantifying these trade-offs, the findings reinforced the value of regression benchmarking as a diagnostic tool rather than as an endpoint (Morsy et al., 2017). The comparative results thus aligned with a broader methodological consensus that interpretable models and advanced learners serve complementary roles: regression establishes explanatory credibility, while complex models enhance prioritization efficiency when validated rigorously.

The calibration and ranking results underscored a key theme in contemporary flood risk research: that model evaluation must reflect decision utility rather than abstract statistical optimization. Earlier flood studies frequently reported overall accuracy or discrimination metrics without examining how predictions would translate into actionable thresholds. The present findings demonstrated that calibration quality and ranking concentration were decisive factors in determining practical usefulness. The fused models' lower calibration error and stronger alignment between predicted scores and observed flood frequencies addressed long-standing concerns about probability misinterpretation in machine-learning-based hazard maps (Feng et al., 2019). The improved precision and recall within the top-ranked fraction of predictions aligned with prior work emphasizing that flood management decisions typically focus on a limited subset of high-risk areas. By explicitly evaluating false-alert burden alongside capture rates, the study echoed earlier calls for workload-aware metrics that balance sensitivity and efficiency. The stability of ranking performance across spatial subsets further strengthened confidence in the models' operational relevance. These results contributed to an emerging evaluation paradigm that treats flood mapping as a prioritization problem under uncertainty, where the value of a model lies in its ability to allocate attention effectively rather than to classify every location perfectly (Manzanera et al., 2016). The findings thus reinforced and extended prior methodological critiques by demonstrating how calibration and ranking metrics can be jointly applied

to assess real-world mapping utility.

The robustness analyses demonstrated that performance gains persisted across diverse spatial and contextual partitions, addressing a central challenge identified in earlier flood susceptibility studies. Many prior models reported strong results under random validation but exhibited degraded performance when applied to new regions or physiographic settings. The sustained performance observed across cross-region, catchment, and terrain-class holdouts indicated that the models learned transferable vulnerability patterns rather than overfitting to localized features (Hopkinson et al., 2016). This result aligned with more recent studies that emphasized spatially explicit validation as essential for credible flood modeling. The consistency of findings across land-cover strata further supported the interpretation that the integrated predictor framework captured fundamental flood drivers applicable across urban, agricultural, and natural landscapes. Earlier research often reported uneven performance across surface types, particularly reduced accuracy in urban settings. The present findings suggested that multimodal fusion mitigated these disparities by jointly representing terrain and surface conditions (Norton et al., 2022). By systematically decomposing errors and demonstrating stability under multiple robustness checks, the study addressed critiques in the literature regarding reproducibility and generalization. The discussion therefore situated the findings within an evolving body of work that prioritizes robustness and contextual validity as key criteria for evaluating flood hazard models. The results collectively supported the conclusion that statistically grounded, multimodal, and rigorously validated models provide a more reliable foundation for flood vulnerability assessment than single-source or weakly validated approaches (Chen et al., 2017).

CONCLUSION

The conclusion of this study consolidated the quantitative evidence that flood hazard and land-surface vulnerability were statistically distinguishable when terrain morphology and surface-condition signatures were modeled together within a structured, decision-utility evaluation framework. The results confirmed that flood risk was concentrated in specific landscape configurations characterized by low relative elevation, reduced slope, and strong hydrologic convergence, patterns that were consistently detectable when LiDAR-derived terrain representations were used to capture microtopographic controls and drainage connectivity. The findings also demonstrated that multispectral indicators contributed additional explanatory value by representing surface runoff potential through vegetation condition, wetness-related signatures, imperviousness intensity, and bare-soil exposure, thereby strengthening vulnerability differentiation beyond terrain-only modeling. Comparative model evaluation showed that fusion-based deep learning approaches produced the most favorable combination of discrimination, calibration quality, and ranking utility, indicating that multi-modal integration improved the concentration of true flood-prone locations in the highest-risk subset of mapped outputs while moderating false-alert burden under operational thresholding. The interpretable regression benchmark provided coherent coefficient directions aligned with hydrologic expectations and served as an auditable reference point for evaluating incremental gains from non-linear ensembles and spatial-context neural models. Reliability and stability checks indicated that grouped construct families exhibited acceptable internal consistency and distributional invariance across validation partitions, supporting reproducible measurement behavior for both terrain and multispectral predictors. Robustness testing across region, catchment, and terrain- and land-cover–stratified partitions showed that performance advantages persisted under spatial generalization constraints, strengthening confidence that learned patterns reflected transferable vulnerability structure rather than localized artifacts. Overall, the study established that flood vulnerability prediction achieved its strongest quantitative performance when hazard was treated as a continuous risk surface, when evaluation emphasized decision-utility metrics alongside conventional discrimination summaries, and when LiDAR microtopography and multispectral surface signatures were combined through disciplined preprocessing, validated fusion strategies, and spatially credible holdout testing.

RECOMMENDATIONS

Recommendations derived from this study focused on strengthening the technical rigor, operational usability, and governance alignment of flood hazard mapping systems that integrate LiDAR and multispectral data through deep learning. First, flood risk products should be reported as continuous

vulnerability surfaces with calibrated probability-like scores, accompanied by clearly defined operational thresholds that align alert volume with institutional capacity for mitigation planning and review. This study's findings indicated that ranking utility and false-alert burden were decisive for practical value, so performance reporting should include top-ranked capture metrics and workload-sensitive summaries in addition to global discrimination measures. Second, preprocessing governance should be treated as part of model validity: LiDAR hydrologic conditioning parameters, multispectral radiometric normalization routines, masking decisions, and co-registration tolerances should be standardized, documented, and version-controlled so that risk surfaces remain reproducible across updates and comparable across jurisdictions. Third, implementation should prioritize multi-modal fusion architectures that preserve spatial context, since the strongest gains were observed when terrain microstructure and surface-condition signatures were jointly represented rather than used in isolation. At the same time, an interpretable benchmark model should be maintained alongside deep learning outputs to support transparency, stakeholder communication, and diagnostic accountability when model behavior is questioned in specific locations. Fourth, evaluation protocols should adopt spatially explicit validation by default, including cross-region and catchment holdouts, and results should be decomposed by terrain class and land-cover regime to identify systematic failure modes and prevent misleading aggregate performance claims. Fifth, operational deployment should incorporate uncertainty-aware reporting, where confidence indicators are provided for areas affected by label ambiguity, cloud contamination, or sensor noise, allowing decision makers to distinguish high-risk zones supported by strong evidence from those requiring additional verification. Sixth, data integration pipelines should include routine checks for temporal alignment between flood-event references and multispectral observations, since partial observability can bias both calibration and apparent detection rates. Finally, adoption should be supported by model governance artifacts, including feature dictionaries, preprocessing logs, calibration reports, and decision-threshold justifications, ensuring audit readiness and enabling consistent interpretation of vulnerability grades across agencies and time periods. These recommendations emphasized disciplined fusion modeling, spatially credible validation, calibrated decision outputs, and traceable workflows as the core requirements for reliable, decision-useful flood hazard and land-surface vulnerability prediction.

LIMITATIONS

Several limitations constrained the interpretation of results produced by this study and defined the boundaries of inference for the reported flood hazard and land-surface vulnerability maps. A primary limitation concerned label quality and partial observability. Flood extent references derived from remote sensing or event archives were subject to temporal misalignment with peak inundation, cloud contamination in optical imagery, and mixed-pixel ambiguity along flood boundaries, which introduced misclassification noise into both training and evaluation targets. This limitation was particularly relevant in vegetated floodplains and dense urban areas where water detection can be obscured by canopy cover, shadowing, or complex surface materials. A second limitation involved spatial autocorrelation and validation dependence. Although spatial holdouts and partition discipline were applied, residual spatial dependence may have remained within partitions due to broad-scale physiographic similarity, meaning that performance metrics could still reflect some degree of spatial familiarity rather than full out-of-area transfer. Third, resolution harmonization introduced methodological constraints. LiDAR and multispectral sources differed in spatial resolution and acquisition geometry, and resampling required to align datasets could have smoothed microtopographic detail or introduced interpolation artifacts, affecting both engineered predictors and learned representations. Fourth, terrain conditioning choices represented an additional source of uncertainty. Sink filling, breaching, and channel enforcement decisions influenced drainage connectivity proxies and convergence features, and alternative conditioning settings could yield materially different vulnerability patterns in flat basins where small barriers govern flow direction. Fifth, multispectral predictors remained sensitive to atmospheric correction and radiometric normalization assumptions. Even under standardized preprocessing, reflectance variability associated with aerosols, seasonal illumination differences, and sensor-specific bandpass characteristics could influence index-based descriptors of wetness, vegetation condition, and built-up intensity. Sixth, model interpretability differed across methods. While regression benchmarking supported transparent

coefficient interpretation, deep learning fusion models relied on latent representations that were less directly attributable to physical mechanisms, limiting explanatory granularity for certain localized predictions.

REFERENCES

[1]. Abdelkarim, A., Al-Alola, S. S., Alogayell, H. M., Mohamed, S. A., Alkadi, I. I., & Ismail, I. Y. (2020). Integration of GIS-based multicriteria decision analysis and analytic hierarchy process to assess flood hazard on the Al-shamal train pathway in Al-Qurayyat region, kingdom of Saudi Arabia. *Water*, *12*(6), 1702.

[2]. Abdul, K. (2023). Artificial Intelligence–Driven Predictive Microbiology in Dairy And Livestock Supply Chains. *International Journal of Scientific Interdisciplinary Research*, *4*(4), 286–335. https://doi.org/10.63125/syj6pp52

[3]. Ahmadlou, M., Al-Fugara, A. k., Al-Shabeeb, A. R., Arora, A., Al-Adamat, R., Pham, Q. B., Al-Ansari, N., Linh, N. T. T., & Sajedi, H. (2021). Flood susceptibility mapping and assessment using a novel deep learning model combining multilayer perceptron and autoencoder neural networks. *Journal of Flood Risk Management*, *14*(1), e12683.

[4]. Akay, H. (2021). Flood hazards susceptibility mapping using statistical, fuzzy logic, and MCDM methods. *Soft Computing*, *25*(14), 9325-9346.

[5]. Al-Ruzouq, R., Shanableh, A., Jena, R., Gibril, M. B. A., Hammouri, N. A., & Lamghari, F. (2024). Flood susceptibility mapping using a novel integration of multi-temporal sentinel-1 data and eXtreme deep learning model. *Geoscience Frontiers*, *15*(3), 101780.

[6]. Antzoulatos, G., Kouloglou, I.-O., Bakratsas, M., Moumtzidou, A., Gialampoukidis, I., Karakostas, A., Lombardo, F., Fiorin, R., Norbiato, D., & Ferri, M. (2022). Flood hazard and risk mapping by applying an explainable machine learning framework using satellite imagery and GIS data. *Sustainability*, *14*(6), 3251.

[7]. Arnell, N. W., & Gosling, S. N. (2016). The impacts of climate change on river flood risk at the global scale. *Climatic Change*, *134*(3), 387-401.

[8]. Baky, M. A. A., Islam, M., & Paul, S. (2020). Flood hazard, vulnerability and risk assessment for different land use classes using a flow model. *Earth Systems and Environment*, *4*(1), 225-244.

[9]. Balestra, M., Marselis, S., Sankey, T. T., Cabo, C., Liang, X., Mokroš, M., Peng, X., Singh, A., Stereńczak, K., & Vega, C. (2024). LiDAR data fusion to improve forest attribute estimates: A review. *Current Forestry Reports*, *10*(4), 281-297.

[10]. Bammou, Y., Benzougagh, B., Igmoullan, B., Kader, S., Ouallali, A., Spalevic, V., Sestras, P., & Kuriqi, A. (2024). Spatial mapping for multi-hazard land management in sparsely vegetated watersheds using machine learning algorithms. *Environmental Earth Sciences*, *83*(15), 447.

[11]. Bathrellos, G. D., Karymbalis, E., Skilodimou, H. D., Gaki-Papanastassiou, K., & Baltas, E. A. (2016). Urban flood hazard assessment in the basin of Athens Metropolitan city, Greece. *Environmental Earth Sciences*, *75*(4), 319.

[12]. Bernard, T. G., Davy, P., & Lague, D. (2022). Hydro-geomorphic metrics for high resolution fluvial landscape analysis. *Journal of Geophysical Research: Earth Surface*, *127*(3), e2021JF006535.

[13]. Boulton, S. J., & Stokes, M. (2018). Which DEM is best for analyzing fluvial landscape development in mountainous terrains? *Geomorphology*, *310*, 168-187.

[14]. Bui, D. T., Hoang, N.-D., Martínez-Álvarez, F., Ngo, P.-T. T., Hoa, P. V., Pham, T. D., Samui, P., & Costache, R. (2020). A novel deep learning neural network approach for predicting flash flood susceptibility: A case study at a high frequency tropical storm area. *Science of the Total Environment*, *701*, 134413.

[15]. Cao, C., Xu, P., Wang, Y., Chen, J., Zheng, L., & Niu, C. (2016). Flash flood hazard susceptibility mapping using frequency ratio and statistical index methods in coalmine subsidence areas. *Sustainability*, *8*(9), 948.

[16]. Chen, B., Shi, S., Gong, W., Zhang, Q., Yang, J., Du, L., Sun, J., Zhang, Z., & Song, S. (2017). Multispectral LiDAR point cloud classification: A two-step approach. *Remote Sensing*, *9*(4), 373.

[17]. Chen, H., Liang, Q., Liu, Y., & Xie, S. (2018). Hydraulic correction method (HCM) to enhance the efficiency of SRTM DEM in flood modeling. *Journal of Hydrology*, *559*, 56-70.

[18]. Costache, R., Arabameri, A., Costache, I., Crăciun, A., Islam, A. R. M. T., Abba, S., Sahana, M., & Pham, B. T. (2022). Flood susceptibility evaluation through deep learning optimizer ensembles and GIS techniques. *Journal of environmental management*, *316*, 115316.

[19]. Costache, R., Ngo, P. T. T., & Bui, D. T. (2020). Novel ensembles of deep learning neural network and statistical learning for flash-flood susceptibility mapping. *Water*, *12*(6), 1549.

[20]. Costache, R., Pal, S. C., Pande, C. B., Islam, A. R. M. T., Alshehri, F., & Abdo, H. G. (2024). Flood mapping based on novel ensemble modeling involving the deep learning, Harris Hawk optimization algorithm and stacking based machine learning. *Applied Water Science*, *14*(4), 78.

[21]. Darabi, H., Choubin, B., Rahmati, O., Haghighi, A. T., Pradhan, B., & Kløve, B. (2019). Urban flood risk mapping using the GARP and QUEST models: A comparative study of machine learning techniques. *Journal of Hydrology*, *569*, 142-154.

[22]. De Moel, H., Jongman, B., Kreibich, H., Merz, B., Penning-Rowsell, E., & Ward, P. J. (2015). Flood risk assessments at different spatial scales. *Mitigation and Adaptation Strategies for Global Change*, *20*(6), 865-890.

[23]. Demir, V., & Kisi, O. (2016). Flood hazard mapping by using geographic information system and hydraulic model: Mert River, Samsun, Turkey. *Advances in Meteorology*, *2016*(1), 4891015.

[24]. Dey, S., Saksena, S., & Merwade, V. (2019). Assessing the effect of different bathymetric models on hydraulic simulation of rivers in data sparse regions. *Journal of Hydrology*, *575*, 838-851.

[25]. Dietrich, A., & Krautblatter, M. (2019). Deciphering controls for debris-flow erosion derived from a LiDAR-recorded extreme event and a calibrated numerical model (Roßbichelbach, Germany). *Earth Surface Processes and Landforms*, *44*(6), 1346-1361.
[26]. Eini, M., Kaboli, H. S., Rashidian, M., & Hedayat, H. (2020). Hazard and vulnerability in urban flood risk mapping: Machine learning techniques and considering the role of urban districts. *International Journal of Disaster Risk Reduction*, *50*, 101687.
[27]. El-Magd, S. A. A., Pradhan, B., & Alamri, A. (2021). Machine learning algorithm for flash flood prediction mapping in Wadi El-Laqeita and surroundings, Central Eastern Desert, Egypt. *Arabian Journal of Geosciences*, *14*(4), 323.
[28]. Emerton, R., Cloke, H., Stephens, E., Zsoter, E., Woolnough, S., & Pappenberger, F. (2017). Complex picture for likelihood of ENSO-driven flood hazard. *Nature communications*, *8*(1), 14796.
[29]. Erena, S. H., Worku, H., & De Paola, F. (2018). Flood hazard mapping using FLO-2D and local management strategies of Dire Dawa city, Ethiopia. *Journal of Hydrology: Regional Studies*, *19*, 224-239.
[30]. Farahmand, H., Xu, Y., & Mostafavi, A. (2023). A spatial–temporal graph deep learning model for urban flood nowcasting leveraging heterogeneous community features. *Scientific Reports*, *13*(1), 6768.
[31]. Feng, Q., Zhu, D., Yang, J., & Li, B. (2019). Multisource hyperspectral and LiDAR data fusion for urban land-use mapping based on a modified two-branch convolutional neural network. *ISPRS International Journal of Geo-Information*, *8*(1), 28.
[32]. Fereshtehpour, M., Esmaeilzadeh, M., Alipour, R. S., & Burian, S. J. (2024). Impacts of DEM type and resolution on deep learning-based flood inundation mapping. *Earth Science Informatics*, *17*(2), 1125-1145.
[33]. Ghamisi, P., Rasti, B., Yokoya, N., Wang, Q., Hofle, B., Bruzzone, L., Bovolo, F., Chi, M., Anders, K., & Gloaguen, R. (2019). Multisource and multitemporal data fusion in remote sensing: A comprehensive review of the state of the art. *IEEE Geoscience and Remote Sensing Magazine*, *7*(1), 6-39.
[34]. Gigović, L., Pamučar, D., Bajić, Z., & Drobnjak, S. (2017). Application of GIS-interval rough AHP methodology for flood hazard mapping in urban areas. *Water*, *9*(6), 360.
[35]. Gori, A., Lin, N., & Xi, D. (2020). Tropical cyclone compound flood hazard assessment: From investigating drivers to quantifying extreme water levels. *Earth's Future*, *8*(12), e2020EF001660.
[36]. Grau, J., Liang, K., Ogilvie, J., Arp, P., Li, S., Robertson, B., & Meng, F.-R. (2021). Using unmanned aerial vehicle and lidar-derived DEMs to estimate channels of small tributary streams. *Remote Sensing*, *13*(17), 3380.
[37]. Gu, Y., Jin, X., Xiang, R., Wang, Q., Wang, C., & Yang, S. (2020). UAV-based integrated multispectral-LiDAR imaging system and data processing. *Science China Technological Sciences*, *63*(7), 1293-1301.
[38]. Haggag, M., Siam, A. S., El-Dakhakhni, W., Coulibaly, P., & Hassini, E. (2021). A deep learning model for predicting climate-induced disasters. *Natural hazards*, *107*(1), 1009-1034.
[39]. Hammad, S., & Md Sarwar Hossain, S. (2025). Advanced Engineering Materials and Performance-Based Design Frameworks For Resilient Rail-Corridor Infrastructure. *International Journal of Scientific Interdisciplinary Research*, *6*(1), 368–403. https://doi.org/10.63125/c3g3sx44
[40]. Hammad, S., & Muhammad Mohiul, I. (2023). Geotechnical And Hydraulic Simulation Models for Slope Stability And Drainage Optimization In Rail Infrastructure Projects. *Review of Applied Science and Technology*, *2*(02), 01–37. https://doi.org/10.63125/jmx3p851
[41]. Hänsch, R., & Hellwich, O. (2020). Fusion of multispectral LiDAR, hyperspectral, and RGB data for urban land cover classification. *IEEE Geoscience and Remote Sensing Letters*, *18*(2), 366-370.
[42]. Hazarika, N., Barman, D., Das, A., Sarma, A., & Borah, S. (2018). Assessing and mapping flood hazard, vulnerability and risk in the Upper Brahmaputra River valley using stakeholders' knowledge and multicriteria evaluation (MCE). *Journal of Flood Risk Management*, *11*, S700-S716.
[43]. Herath, M., Jayathilaka, T., Hoshino, Y., & Rathnayake, U. (2023). Deep machine learning-based water level prediction model for Colombo flood detention area. *Applied Sciences*, *13*(4), 2194.
[44]. Hopkinson, C., Chasmer, L., Gynan, C., Mahoney, C., & Sitar, M. (2016). Multisensor and multispectral LiDAR characterization and classification of a forest environment. *Canadian journal of remote sensing*, *42*(5), 501-520.
[45]. Ighile, E. H., Shirakawa, H., & Tanikawa, H. (2022). Application of GIS and machine learning to predict flood areas in Nigeria. *Sustainability*, *14*(9), 5039.
[46]. Jabed Hasan, T., & Waladur, R. (2023). AI-Driven Cybersecurity, IOT Networking, And Resilience Strategies For Industrial Control Systems: A Systematic Review For U.S. Critical Infrastructure Protection. *International Journal of Scientific Interdisciplinary Research*, *4*(4), 144–176. https://doi.org/10.63125/mbyhj941
[47]. Jinnat, A., & Md. Kamrul, K. (2021). LSTM and GRU-Based Forecasting Models For Predicting Health Fluctuations Using Wearable Sensor Streams. *American Journal of Interdisciplinary Studies*, *2*(02), 32-66. https://doi.org/10.63125/1p8gbp15
[48]. Johnson, F., White, C. J., van Dijk, A., Ekstrom, M., Evans, J. P., Jakob, D., Kiem, A. S., Leonard, M., Rouillard, A., & Westra, S. (2016). Natural hazards in Australia: floods. *Climatic Change*, *139*(1), 21-35.
[49]. Kabenge, M., Elaru, J., Wang, H., & Li, F. (2017). Characterizing flood hazard risk in data-scarce areas, using a remote sensing and GIS-based flood hazard index. *Natural hazards*, *89*(3), 1369-1387.
[50]. Karyotis, C., Maniak, T., Doctor, F., Iqbal, R., Palade, V., & Tang, R. (2019). Deep learning for flood forecasting and monitoring in urban environments. 2019 18th IEEE International Conference On Machine Learning And Applications (ICMLA),
[51]. Kazakis, N., Kougias, I., & Patsialis, T. (2015). Assessment of flood hazard areas at a regional scale using an index-based approach and Analytical Hierarchy Process: Application in Rhodope–Evros region, Greece. *Science of the Total Environment*, *538*, 555-563.

[52]. Kumar, R., & Acharya, P. (2016). Flood hazard and risk assessment of 2014 floods in Kashmir Valley: a space-based multisensor approach. *Natural hazards*, *84*(1), 437-464.
[53]. Kundzewicz, Z. W., Krysanova, V., Dankers, R., Hirabayashi, Y., Kanae, S., Hattermann, F. F., Huang, S., Milly, P. C., Stoffel, M., & Driessen, P. (2017). Differences in flood hazard projections in Europe–their causes and consequences for decision making. *Hydrological Sciences Journal*, *62*(1), 1-14.
[54]. Kvočka, D., Falconer, R. A., & Bray, M. (2016). Flood hazard assessment for extreme flood events. *Natural hazards*, *84*(3), 1569-1599.
[55]. Lay, U. S., Pradhan, B., Yusoff, Z. B. M., Abdallah, A. F. B., Aryal, J., & Park, H.-J. (2019). Data mining and statistical approaches in debris-flow susceptibility modelling using airborne LiDAR data. *Sensors*, *19*(16), 3451.
[56]. Lee, C.-C., & Gharaibeh, N. G. (2022). Assessing surface drainage conditions at the street and neighborhood scale: A computer vision and flow direction method applied to lidar data. *Computers, Environment and Urban Systems*, *93*, 101755.
[57]. Linardos, V., Drakaki, M., Tzionas, P., & Karnavas, Y. L. (2022). Machine learning in disaster management: recent developments in methods and applications. *Machine Learning and Knowledge Extraction*, *4*(2).
[58]. Lindsay, J. B., Francioni, A., & Cockburn, J. M. (2019). LiDAR DEM smoothing and the preservation of drainage features. *Remote Sensing*, *11*(16), 1926.
[59]. Liu, R., Chen, Y., Wu, J., Gao, L., Barrett, D., Xu, T., Li, L., Huang, C., & Yu, J. (2016). Assessing spatial likelihood of flooding hazard using naïve Bayes and GIS: a case study in Bowen Basin, Australia. *Stochastic environmental research and risk assessment*, *30*(6), 1575-1590.
[60]. Luppichini, M., Barsanti, M., Giannecchini, R., & Bini, M. (2022). Deep learning models to predict flood events in fast-flowing watersheds. *Science of the Total Environment*, *813*, 151885.
[61]. Lyu, H.-M., Wang, G.-F., Shen, J. S., Lu, L.-H., & Wang, G.-Q. (2016). Analysis and GIS mapping of flooding hazards on 10 May 2016, Guangzhou, China. *Water*, *8*(10), 447.
[62]. Macchione, F., Costabile, P., Costanzo, C., & De Santis, R. (2019). Moving to 3-D flood hazard maps for enhancing risk communication. *Environmental modelling & software*, *111*, 510-522.
[63]. Manfreda, S., Samela, C., Gioia, A., Consoli, G. G., Iacobellis, V., Giuzio, L., Cantisani, A., & Sole, A. (2015). Flood-prone areas assessment using linear binary classifiers based on flood maps obtained from 1D and 2D hydraulic models. *Natural hazards*, *79*(2), 735-754.
[64]. Manzanera, J. A., García-Abril, A., Pascual, C., Tejera, R., Martín-Fernández, S., Tokola, T., & Valbuena, R. (2016). Fusion of airborne LiDAR and multispectral sensors reveals synergic capabilities in forest structure characterization. *GIScience & Remote Sensing*, *53*(6), 723-738.
[65]. Maranzoni, A., D'Oria, M., & Rizzo, C. (2023). Quantitative flood hazard assessment methods: A review. *Journal of Flood Risk Management*, *16*(1), e12855.
[66]. Masud, R., & Md Sarwar Hossain, S. (2024). The Impact of Smart Materials And Fire-Resistant Structures On Safety In U.S. Public Infrastructure. *Journal of Sustainable Development and Policy*, *3*(03), 44-86. https://doi.org/10.63125/ygr1yk30
[67]. Md, K., & Sai Praveen, K. (2024). Hybrid Discrete-Event And Agent-Based Simulation Framework (H-DEABSF) For Dynamic Process Control In Smart Factories. *ASRC Procedia: Global Perspectives in Science and Scholarship*, *4*(1), 72–96. https://doi.org/10.63125/wcqq7x08
[68]. Md Nahid, H., & Tahmina Akter Bhuya, M. (2024). An Empirical Study of Big Data–Enabled Predictive Analytics And Their Impact On Financial Forecasting And Market Decision-Making. *Review of Applied Science and Technology*, *3*(01), 143–182. https://doi.org/10.63125/1mjfqf10
[69]. Md Newaz, S., & Md Jahidul, I. (2024). AI-Powered Business Analytics For Smart Manufacturing And Supply Chain Resilience. *Review of Applied Science and Technology*, *3*(01), 183–220. https://doi.org/10.63125/va5gpg60
[70]. Md. Akbar, H. (2024). Computational Psychometrics and Digital Biomarker Modeling For Precision Mental Health Diagnostics. *International Journal of Scientific Interdisciplinary Research*, *5*(2), 487–525. https://doi.org/10.63125/vg522x27
[71]. Md. Akbar, H., & Sharmin, A. (2022). Neurobiotechnology-Driven Regenerative Therapy Frameworks For Post-Traumatic Neural Recovery. *American Journal of Scholarly Research and Innovation*, *1*(02), 134–170. https://doi.org/10.63125/24s6kt66
[72]. Md. Foysal, H., & Subrato, S. (2022). Data-Driven Process Optimization in Automotive Manufacturing A Machine Learning Approach To Waste Reduction And Quality Improvement. *Journal of Sustainable Development and Policy*, *1*(02), 87-133. https://doi.org/10.63125/2hk0qd38
[73]. Md. Mosheur, R. (2025). AI-Driven Predictive Analytics Models For Enhancing Group Insurance Portfolio Performance And Risk Forecasting. *International Journal of Scientific Interdisciplinary Research*, *6*(2), 39–87. https://doi.org/10.63125/qh5qgk22
[74]. Md. Rabiul, K., & Khairul Alam, T. (2024). Impact Of IOT and Blockchain Integration On Real-Time Supply Chain Transparency. *International Journal of Scientific Interdisciplinary Research*, *5*(2), 449–486. https://doi.org/10.63125/2yc6e230
[75]. Melgar-García, L., Martínez-Álvarez, F., Tien Bui, D., & Troncoso, A. (2023). A novel semantic segmentation approach based on U-Net, WU-Net, and U-Net++ deep learning for predicting areas sensitive to pluvial flood at tropical area. *International Journal of Digital Earth*, *16*(1), 3661-3679.
[76]. Mia, M. U., Rahman, M., Elbeltagi, A., Abdullah-Al-Mahbub, M., Sharma, G., Islam, H. T., Pal, S. C., Costache, R., Islam, A. R. M. T., & Islam, M. M. (2022). Sustainable flood risk assessment using deep learning-based algorithms with a blockchain technology. *Geocarto International*, 1-29.

[77]. Mignot, E., Li, X., & Dewals, B. (2019). Experimental modelling of urban flooding: A review. *Journal of Hydrology*, *568*, 334-342.
[78]. Mihu-Pintilie, A., Cîmpianu, C. I., Stoleriu, C. C., Pérez, M. N., & Paveluc, L. E. (2019). Using high-density LiDAR data and 2D streamflow hydraulic modeling to improve urban flood hazard maps: A HEC-RAS multi-scenario approach. *Water*, *11*(9), 1832.
[79]. Moftakhari, H., Schubert, J. E., AghaKouchak, A., Matthew, R. A., & Sanders, B. F. (2019). Linking statistical and hydrodynamic modeling for compound flood hazard assessment in tidal channels and estuaries. *Advances in Water Resources*, *128*, 28-38.
[80]. Moftakhari, H. R., AghaKouchak, A., Sanders, B. F., & Matthew, R. A. (2017). Cumulative hazard: The case of nuisance flooding. *Earth's Future*, *5*(2), 214-223.
[81]. Moishin, M., Deo, R. C., Prasad, R., Raj, N., & Abdulla, S. (2021). Designing deep-based learning flood forecast model with ConvLSTM hybrid algorithm. *Ieee Access*, *9*, 50982-50993.
[82]. Morsy, S., Shaker, A., & El-Rabbany, A. (2017). Multispectral LiDAR data for land cover classification of urban areas. *Sensors*, *17*(5), 958.
[83]. Nandi, A., Mandal, A., Wilson, M., & Smith, D. (2016). Flood hazard mapping in Jamaica using principal component analysis and logistic regression. *Environmental Earth Sciences*, *75*(6), 465.
[84]. Nguyen, P., Thorstensen, A., Sorooshian, S., Hsu, K., AghaKouchak, A., Sanders, B., Koren, V., Cui, Z., & Smith, M. (2016). A high resolution coupled hydrologic–hydraulic model (HiResFlood-UCI) for flash flood modeling. *Journal of Hydrology*, *541*, 401-420.
[85]. Norton, C. L., Hartfield, K., Collins, C. D. H., van Leeuwen, W. J., & Metz, L. J. (2022). Multi-temporal LiDAR and hyperspectral data fusion for classification of semi-arid woody cover species. *Remote Sensing*, *14*(12), 2896.
[86]. O'Neil, G. L., Saby, L., Band, L. E., & Goodall, J. L. (2019). Effects of LiDAR DEM smoothing and conditioning techniques on a topography-based wetland identification model. *Water Resources Research*, *55*(5), 4343-4363.
[87]. Orton, P. M., Hall, T., Talke, S. A., Blumberg, A. F., Georgas, N., & Vinogradov, S. (2016). A validated tropical-extratropical flood hazard assessment for N ew Y ork H arbor. *Journal of Geophysical Research: Oceans*, *121*(12), 8904-8929.
[88]. Oulahen, G., Mortsch, L., Tang, K., & Harford, D. (2015). Unequal vulnerability to flood hazards:"ground truthing" a social vulnerability index of five municipalities in Metro Vancouver, Canada. *Annals of the Association of American Geographers*, *105*(3), 473-495.
[89]. Panahi, M., Jaafari, A., Shirzadi, A., Shahabi, H., Rahmati, O., Omidvar, E., Lee, S., & Bui, D. T. (2021). Deep learning neural networks for spatially explicit prediction of flash flood probability. *Geoscience Frontiers*, *12*(3), 101076.
[90]. Panfilova, T., Kukartsev, V., Tynchenko, V., Tynchenko, Y., Kukartseva, O., Kleshko, I., Wu, X., & Malashin, I. (2024). Flood susceptibility assessment in urban areas via deep neural network approach. *Sustainability*, *16*(17), 7489.
[91]. Papaioannou, G., Vasiliades, L., & Loukas, A. (2015). Multi-criteria analysis framework for potential flood prone areas mapping. *Water resources management*, *29*(2), 399-418.
[92]. Pearson, R. A., Smart, G., Wilkins, M., Lane, E., Harang, A., Bosserelle, C., Cattoën, C., & Measures, R. (2023). GeoFabrics 1.0. 0: An open-source Python package for automatic hydrological conditioning of digital elevation models for flood modelling. *Environmental modelling & software*, *170*, 105842.
[93]. Petrasova, A., Mitasova, H., Petras, V., & Jeziorska, J. (2017). Fusion of high-resolution DEMs for water flow modeling. *Open Geospatial Data, Software and Standards*, *2*(1), 6.
[94]. Pinel, S., Bonnet, M.-P., Santos Da Silva, J., Moreira, D., Calmant, S., Satgé, F., & Seyler, F. (2015). Correction of interferometric and vegetation biases in the SRTMGL1 spaceborne DEM with hydrological conditioning towards improved hydrodynamics modeling in the Amazon Basin. *Remote Sensing*, *7*(12), 16108-16130.
[95]. Prior, E. M., Michaelson, N., Czuba, J. A., Pingel, T. J., Thomas, V. A., & Hession, W. C. (2024). Lidar DEM and computational mesh grid resolutions modify roughness in 2D hydrodynamic models. *Water Resources Research*, *60*(7), e2024WR037165.
[96]. Qiang, Y. (2019). Disparities of population exposed to flood hazards in the United States. *Journal of environmental management*, *232*, 295-304.
[97]. Rallapalli, S., Drewitz, M., Magner, J., Singh, A. P., & Goonetilleke, A. (2022). Hydro-conditioning: advanced approaches for cost-effective water quality management in agricultural watersheds. *Water Research*, *220*, 118647.
[98]. Rana, M., Patel, D., Vakharia, V., & Singh, S. K. (2024). UAV-based DEM augmentation using ConSinGAN for efficient flood parameter prediction with machine learning and 1D hydrodynamic models. *Physics and Chemistry of the Earth, Parts A/B/C*, *135*, 103675.
[99]. Rifat, C., & Rebeka, S. (2023). The Role Of ERP-Integrated Decision Support Systems In Enhancing Efficiency And Coordination In Healthcare Logistics: A Quantitative Study. *International Journal of Scientific Interdisciplinary Research*, *4*(4), 265–285. https://doi.org/10.63125/c7srk144
[100]. Rocha, J., Duarte, A., Fabres, S., Quintela, A., & Serpa, D. (2022). Influence of DEM resolution on the hydrological responses of a terraced catchment: An exploratory modelling approach. *Remote Sensing*, *15*(1), 169.
[101]. Rocha, J., Duarte, A., Silva, M., Fabres, S., Vasques, J., Revilla-Romero, B., & Quintela, A. (2020). The importance of high resolution digital elevation models for improved hydrological simulations of a mediterranean forested catchment. *Remote Sensing*, *12*(20), 3287.
[102]. Rong, Y., Zhang, T., Zheng, Y., Hu, C., Peng, L., & Feng, P. (2020). Three-dimensional urban flood inundation simulation based on digital aerial photogrammetry. *Journal of Hydrology*, *584*, 124308.

[103]. Saharia, M., Kirstetter, P.-E., Vergara, H., Gourley, J. J., & Hong, Y. (2017). Characterization of floods in the United States. *Journal of Hydrology*, *548*, 524-535.
[104]. Sai Praveen, K. (2024). AI-Enhanced Data Science Approaches For Optimizing User Engagement In U.S. Digital Marketing Campaigns. *Journal of Sustainable Development and Policy*, *3*(03), 01-43. https://doi.org/10.63125/65ebsn47
[105]. Saleem, N., Huq, M. E., Twumasi, N. Y. D., Javed, A., & Sajjad, A. (2019). Parameters derived from and/or used with digital elevation models (DEMs) for landslide susceptibility mapping and landslide risk assessment: a review. *ISPRS International Journal of Geo-Information*, *8*(12), 545.
[106]. Santos, P. P., Pereira, S., Zêzere, J. L., Tavares, A. O., Reis, E., Garcia, R. A., & Oliveira, S. C. (2020). A comprehensive approach to understanding flood risk drivers at the municipal level. *Journal of environmental management*, *260*, 110127.
[107]. Satarzadeh, E., Sarraf, A., Hajikandi, H., & Sadeghian, M. S. (2022). Flood hazard mapping in western Iran: assessment of deep learning vis-à-vis machine learning models. *Natural hazards*, *111*(2), 1355-1373.
[108]. Schubert, J. E., Burns, M. J., Fletcher, T. D., & Sanders, B. F. (2017). A framework for the case-specific assessment of Green Infrastructure in mitigating urban flood hazards. *Advances in Water Resources*, *108*, 55-68.
[109]. Shahabi, A., & Tahvildari, N. (2024). A deep-learning model for rapid spatiotemporal prediction of coastal water levels. *Coastal Engineering*, *190*, 104504.
[110]. Shoflul Azam, T., & Md. Al Amin, K. (2024). Quantitative Study on Machine Learning-Based Industrial Engineering Approaches For Reducing System Downtime In U.S. Manufacturing Plants. *International Journal of Scientific Interdisciplinary Research*, *5*(2), 526–558. https://doi.org/10.63125/kr9r1r90
[111]. Slater, L. J., Singer, M. B., & Kirchner, J. W. (2015). Hydrologic versus geomorphic drivers of trends in flood hazard. *Geophysical Research Letters*, *42*(2), 370-376.
[112]. Teng, J., Vaze, J., Kim, S., Dutta, D., Jakeman, A., & Croke, B. (2019). Enhancing the capability of a simple, computationally efficient, conceptual flood inundation model in hydrologically complex terrain. *Water resources management*, *33*(2), 831-845.
[113]. Thapa, S., Shrestha, A., Lamichhane, S., Adhikari, R., & Gautam, D. (2020). Catchment-scale flood hazard mapping and flood vulnerability analysis of residential buildings: The case of Khando River in eastern Nepal. *Journal of Hydrology: Regional Studies*, *30*, 100704.
[114]. Toosi, A. S., Calbimonte, G. H., Nouri, H., & Alaghmand, S. (2019). River basin-scale flood hazard assessment using a modified multi-criteria decision analysis approach: A case study. *Journal of Hydrology*, *574*, 660-671.
[115]. Uddin, K., & Matin, M. A. (2021). Potential flood hazard zonation and flood shelter suitability mapping for disaster risk mitigation in Bangladesh using geospatial technology. *Progress in disaster science*, *11*, 100185.
[116]. Wang, Z., Lai, C., Chen, X., Yang, B., Zhao, S., & Bai, X. (2015). Flood hazard risk assessment model based on random forest. *Journal of Hydrology*, *527*, 1130-1141.
[117]. Wong, J. S., Freer, J. E., Bates, P. D., Warburton, J., & Coulthard, T. J. (2021). Assessing the hydrological and geomorphic behaviour of a landscape evolution model within a limits-of-acceptability uncertainty analysis framework. *Earth Surface Processes and Landforms*, *46*(10), 1981-2003.
[118]. Woodrow, K., Lindsay, J. B., & Berg, A. A. (2016). Evaluating DEM conditioning techniques, elevation source data, and grid resolution for field-scale hydrological parameter extraction. *Journal of Hydrology*, *540*, 1022-1029.
[119]. Wu, D., Li, R., Edidem, M., & Wang, G. (2024). Enhancing hydrologic LiDAR digital elevation models: Bridging hydrographic gaps at fine scales. *JAWRA Journal of the American Water Resources Association*, *60*(6), 1253-1269.
[120]. Yosri, A., Ghaith, M., & El-Dakhakhni, W. (2024). Deep learning rapid flood risk predictions for climate resilience planning. *Journal of Hydrology*, *631*, 130817.
[121]. Youssef, A. M., Pradhan, B., Dikshit, A., & Mahdi, A. M. (2022). Comparative study of convolutional neural network (CNN) and support vector machine (SVM) for flood susceptibility mapping: a case study at Ras Gharib, Red Sea, Egypt. *Geocarto International*, *37*(26), 11088-11115.
[122]. Zaharia, L., Costache, R., Prăvălie, R., & Ioana-Toroimac, G. (2017). Mapping flood and flooding potential indices: a methodological approach to identifying areas susceptible to flood and flooding risk. Case study: the Prahova catchment (Romania). *Frontiers of Earth Science*, *11*(2), 229-247.
[123]. Zhang, W., Liu, Y., Tang, W., Chen, S., & Xie, W. (2023). Rapid spatio-temporal prediction of coastal urban floods based on deep learning approaches. *Urban Climate*, *52*, 101716.
[124]. Zulqarnain, F. N. U. (2022). Policy Optimization for Sustainable Energy Security: Data-Driven Comparative Analysis Between The U.S. And South Asia. *American Journal of Interdisciplinary Studies*, *3*(04), 294-331. https://doi.org/10.63125/v4e4m413
[125]. Zulqarnain, F. N. U., & Subrato, S. (2021). Modeling Clean-Energy Governance Through Data-Intensive Computing And Smart Forecasting Systems. *International Journal of Scientific Interdisciplinary Research*, *2*(2), 128–167. https://doi.org/10.63125/wnd6qs51
[126]. Zulqarnain, F. N. U., & Subrato, S. (2023). Intelligent Climate Risk Modeling For Robust Energy Resilience And National Security. *Journal of Sustainable Development and Policy*, *2*(04), 218-256. https://doi.org/10.63125/jmer2r39